Aalto University
School of Science
Master's Programme in Engineering Physics

Janika Tang

Sensitivity analysis of the probabilistic seismic hazard assessment on the Hanhikivi site

Master's Thesis
Espoo, September 27, 2019

Supervisor: Professor Filip Tuomisto
Advisor: Juho Helander, M.Sc. (Tech.)

Aalto University
School of Science
Master's Programme in Engineering Physics

ABSTRACT OF
MASTER'S THESIS

Author: Janika Tang

Title:
Sensitivity analysis of the probabilistic seismic hazard assessment on the Hanhikivi site

Date:	September 27, 2019	**Pages:**	46+25
Major:	Engineering physics	**Code:**	SCI3056
Supervisor:	Professor Filip Tuomisto		
Advisor:	Juho Helander, M.Sc. (Tech.)		

Nuclear energy company Fennovoima is planning to construct a nuclear power plant (NPP) on the Hanhikivi peninsula in Pyhäjoki. Prior to construction, the Hanhikivi 1 NPP shall be designed to withstand seismic hazards. In the Finnish nuclear industry, the assessment of seismic risks begins with a probabilistic seismic hazard assessment (PSHA) [1]. The aim of this work is to review the most significant parameters in the logic tree of Hanhikivi 1 PSHA. The scope of the thesis includes examining approaches to evaluate the maximum magnitude ($m_{\max}$) and involving two new ground motion prediction equations (GMPEs) in the PSHA. We corrected the weights calculated by applying the Kijko approach in the current PSHA and demonstrated the shortcomings of the weight assessment method. We also attempted to derive the $m_{\max}$ directly from the Kijko approach, but the calculated value was deemed unreasonably low. The first included GMPE was the modified G16 GMPE recently developed to the Fennoscandian conditions [2]. The second GMPE was derived from the Dahle function [3] by the author. The modified Dahle GMPE was calibrated to Fennoscandia in the applicability range of $R_{\text{hyp}} \leq 200$ km and $M_w \leq 6{,}5$. A comparison to the measured data and the other GMPEs suggests that the modified Dahle GMPE underestimates ground motion for $M_w < 5,0$ in near distance ($R_{\text{hyp}} \leq 10$ km). Therefore, we included the modified Dahle GMPE in the logic tree with a relatively small weight factor. We ran the seismic hazard analyses on EZ-FRISK and compiled the ground response spectra (GRS) following the logic tree. The GRS were compiled for a range of annual frequencies of exceedance (AFE = 10^{-4} a^{-1} - 10^{-8} a^{-1}), but the thesis only discusses the results at AFE = 10^{-5} a^{-1} due to its significance in nuclear safety. We compared the computed GRS with the current GRS of the Hanhikivi 1 site. Including the new GMPEs alleviated the unphysical features in the current Hanhikivi 1 GRS caused by the drastically different ranges of the Pezeshk and Fennoscandian GMPEs. In summary, we improved our understanding of the PSHA sensitivity to the $m_{\max}$ and GMPE parameters, but our work also brought up and highlighted issues regarding them.

Keywords: probabilistic seismic hazard assessment, ground motion prediction, magnitude, nuclear safety, seismology

Language: English

Aalto-yliopisto
Perustieteiden korkeakoulu
Teknillisen fysiikan maisteriohjelma

DIPLOMITYÖN
TIIVISTELMÄ

Tekijä: Janika Tang

Työn nimi:
Probabilistisen seismisen hasardilaskennan herkkyystarkastelu Hanhikiven laitospaikalla

Päiväys:	27. syyskuuta 2019	**Sivumäärä:**	46+25
Pääaine:	Teknillinen fysiikka	**Koodi:**	SCI3056
Valvoja:	Professori Filip Tuomisto		
Ohjaaja:	DI Juho Helander		

Energiayhtiö Fennovoima suunnittelee ydinvoimalaitoksen rakentamista Hanhikivenniemelle Pyhäjoella. Rakentamislupaa varten voimalaitos täytyy suunnitella kestämään seismisiä hasardeja. Suomessa seismisten riskien arviointiin käytetään todennäköisyysperusteista seismisen hasardin arviointia (PSHA). Työssä on tarkoituksena tarkastella Hanhikivi 1 -laitoksen PSHA:n logiikkapuun merkittävimpien parametrien laskentaa. Lisäksi työssä käydään läpi tapoja maksimimagnitudin ($m_{\max}$) määrittämiseen ja lisätään kaksi uutta maanvaimennusyhtälöä (GMPE) logiikkapuuhun. Työssä korjattiin tämänhetkisen PSHA:n väärinlasketut Kijko-menetelmään pohjautuvat painokertoimet ja demonstroitiin painotusten laskemistavan heikkouksia. Maksimimagnitudi yritettiin määrittää myös suoraan Kijko-menetelmästä, mutta tulos oli epäuskottavan pieni. Logiikkapuun ensimmäinen uusi GMPE on vastikään Fennoskandian oloihin kehitelty muunnettu G16 GMPE [2]. Toinen GMPE johdettiin Dahle-funktiosta [3] osana diplomityötä. Muunnettu Dahle GMPE kalibroitiin Fennoskandian oloihin, jossa sen on arvioitu soveltuvan $R_{\text{hyp}} \leq 200$ km ja $M_w \leq 6{,}5$ välillä. Muunnettua Dahle GMPE:tä vertailtiin mittauksiin ja muihin GMPE:ihin, minkä perusteella GMPE vaikuttaa aliarvioivan maanliikettä matalilla magnitudeilla $M_w < 5{,}0$ lähietäisyydellä ($R_{\text{hyp}} \leq 10$ km). Muunnettu Dahle GMPE sisällytettiin silti logiikkapuuhun, mutta pienemmällä painokertoimella. Seismiset hasardianalyysit ajettiin EZ-FRISK-ohjelmistolla, ja hasardianalyyseistä koostettiin logiikkapuuta vastaavat maavastespektrit. Maavastespektrit koostettiin usealle esiintymistaajuudelle (AFE = 10^{-4} a^{-1} - 10^{-8} a^{-1}), mutta työssä keskitytään esiintymistaajuuteen AFE = 10^{-5} a^{-1} taajuuden turvallisuusmerkityksen vuoksi. Vertasimme laskettua maavastespektriä nykyiseen Hanhikivi 1 laitoksen maavastespektriin. Uusien GMPE:iden läsnäolo vähensi nykyisessä Hanhikivi 1 -maavastespektrissä havaittuja epäfysikaalisia piirteitä. Yhteenvetona työ paransi ymmärrystä PSHA:n herkkyydstä $m_{\max}$- ja GMPE-parametreille, mutta työssä tuotiin esiin myös ongelmat parametreihin liittyen.

Asiasanat:	todennäköisyysperusteinen seisminen hasardiarvio, maanvaimennusyhtälö, magnitudi, ydinturvallisuus, seismologia
Kieli:	Englanti

Acknowledgements

This thesis would have been very difficult without certain people. I wish to thank my thesis instructor Juho Helander for the advice given during the writing process and professor Filip Tuomisto for his guidance over the course of my M.Sc. studies. I also want to thank Dr. Jussi Kumpula for the computational resources and the proof-reading. Lastly, I want to thank Calle Korhonen for his support during my internship.

Helsinki, September 27, 2019

Janika Tang

Contents

Common symbols and abbreviations

Symbols

β	Gutenberg-Richter parameter
d	Earthquake depth
f	Frequency
$f(x)$	Probability distribution function of variable x
$F(x)$	Cumulative distribution function of variable x
λ	Seismic activity rate
$m_{\max}$	Maximum magnitude
$m_{\max}^{\text{obs}}$	Maximum observed magnitude
M_w	Moment magnitude
$\mathcal{N}(\mu, \sigma_\mu^2)$	Normal distribution with mean μ and variance σ_μ^2
R_{ep}	Epicentral distance
R_{hyp}	Hypocentral distance
σ_x	Standard deviation of variable x
$\bar{Y}_{\text{GMPE}}$	Median ground motion
v_{s30}	Shear wave velocity for the upper 30 m depth

Abbreviations

AFE	Annual frequency of exceedance
CENA	Central & Eastern North-America
DBE	Design basis earthquake
DEC	Design extension conditions
FGMPE	Fennoscandian ground motion prediction equation
GM	Ground motion
GMPE	Ground motion prediction equation
GR	Gutenberg-Richter
GRS	Ground response spectrum
NPP	Nuclear power plant
PGA	Peak ground acceleration
PSHA	Probabilistic seismic hazard assessment
SA	Spectral acceleration
STUK	Radiation and Nuclear Safety Authority in Finland
VTT	VTT Technical Research Centre of Finland Ltd
YVL	Regulatory guides on nuclear safety

Chapter 1

Introduction

Fennovoima is planning to construct a new nuclear power plant (NPP) at the Hanhikivi site in Pyhäjoki, Northern Ostrobothnia. Prior to construction, the Hanhikivi 1 NPP shall be designed to withstand a variety of external hazards that may challenge safety functions [4]. A major external hazard to be considered is the possibility of earthquakes. Fennoscandia is generally regarded as an area of low seismic risk, but earthquakes of considerable sizes still occur. As a case in point, an earthquake of magnitude M4,1 was recently measured in the Bothnian Bay roughly 100 km from the Hanhikivi site. Although the earthquake was exceptionally large in Fennoscandia, similar events are taken in the account in the NPP design [5].

In light of this, the YVL guide B.7 [1] requires the seismic hazard to be considered in the design of the NPP. The design basis earthquake (DBE) shall be determined by probabilistic seismic hazard assessment (PSHA) and the external impact to the NPP shall be presented as a ground response spectrum (GRS). In addition to the DBE, the design extension condition (DEC) C earthquake shall also be determined. In a DEC C event, the plant shall be demonstrated to reach the controlled state and subsequently the safe state. However, the YVL guide does not precisely state the acceptable methods for PSHA. As the nuclear energy industry is the only field in Finland requiring seismic planning, much of the methodology is developed by the industry itself.

As a result, Fennovoima has conducted several studies to assess the seismic hazard at the Hanhikivi 1 site. The preliminary work began as early as in 2008 to evaluate alternative plant sites [6–8]. In 2011, Fennovoima announced the plant would be built on the Hanhikivi site in Pyhäjoki [9]. Following this,

STUK requested additional studies to reduce uncertainties in seismic hazard assessment [10]. In response, Fennovoima conducted an extensive project between 2013 - 2015 to assess the seismic hazard at the Hanhikivi site region [11]. The project resulted in two reports [11, 12] that updated every aspect of PSHA replacing the earlier reports completely. Afterwards, an error was found in processing ground motion [13] and corrected [14], and the ground response spectra were updated [15–17].

The most challenging task in conducting a PSHA is determining the parameters defining the seismicity and the attenuation characteristics in the area of interest. The seismicity is expressed as a seismotectonic model consisting of seismic source areas with given seismic activity rate and magnitude-frequency relation. The attenuation characteristics are described in a form of ground motion prediction equation (GMPE) defining the attenuation of a seismic wave traveling from source to site.

In this work, we review the Hanhikivi 1 PSHA focusing on the GMPE and the maximum magnitude. We derive a new Dahle-based GMPE calibrated with the Fennoscandian and North American measurements and include it in the Hanhikivi 1 PSHA. In addition, we include the modified G16 GMPE introduced by Fülöp et al. (2019) [2]. We also revise the current approach to assess maximum magnitudes and examine alternative approaches. The structure of the thesis is as follows. Chapter 2 gives a brief background of the PSHA in general and regarding the Hanhikivi 1 NPP site. Chapter 3 presents the theoretical background of the maximum magnitude assessment, ground motion prediction and seismic hazard calculation. Sections 4.1 - 4.2 describe the calibration of the modified Dahle GMPE and compare the GMPEs. In sections 4.3 - 4.4, we describe the weight assessment of the logic tree parameters and present the computational parameters. Finally, chapter 5 examines the computed ground response spectra while chapter 6 concludes the thesis.

Chapter 2

Background

In the nuclear industry, the assessment of seismic risks begins with a seismic hazard assessment [18]. The International Atomic Energy Agency's (IAEA) [18] guide on seismic hazard assessment presents the probabilistic seismic hazard assessment in five main steps (direct quote):

1. Evaluation of the seismotectonic model for the site region in terms of the defined seismic sources, including uncertainty in their boundaries and dimensions
2. For each seismic source, evaluation of the maximum potential magnitude, the rate of earthquake occurrence and the type of magnitude-frequency relationship, together with the uncertainty associated with each evaluation.
3. Selection of the attenuation relationships for the site region, and assessment of the uncertainty in both the mean and the variability of the ground motion as a function of earthquake magnitude and seismic source to site distance.
4. Performance of the hazard calculation.
5. Taking account of the site response.

Evaluation of the seismotectonic model in step 1 forms the foundation for the seismic hazard assessment. A seismotectonic model divides the area of interest into seismic source areas (SSAs) based on their different seismicity patterns and tectonic history [12]. Korja and Kosonen (2015) [12] defined two seismotectonic models for the Hanhikivi 1 site with both of them comprising an area of a 500 km radius around the Hanhikivi 1 site. Model 1

was consructed based on the potential reactivation of geologically ancient features while Model 2 is based on the analysis of recently active structures. Korja and Kosonen (2015) [12] also defined the rate of earthquake occurrence and the Gutenberg-Richter (GR) parameter, namely the seismic activity parameters in step 2, for the SSAs. The GR parameter defines the magnitude-frequency relation through the GR equation commonly applied in PSHA [18]. In addition, we must also define the depth range considered in the seismic calculations. The PSHAs conducted with the current seismotectonic models [11, 15–17] have adapted a depth range of d = 0 - 45 km based on the average crustal depth in the area [11]. Saari et al. (2015) conducted a sensitivity study with d = 0 - 30 km, since it was concluded to cover the seismogenic layer, where 99% of the earthquakes occur [12]. The larger depth range overestimates the possibility of very shallow large earthquakes and very deep earthquakes [19]. The study conducted for the PGA at an annual frequency of exceedance of 10^{-5} a^{-1} found decreasing the depth range to increase the median by nearly 10%, a low number considering the overall uncertainty.

The magnitude-frequency relationship is strongly affected by the maximum magnitude. The first PSHAs performed for the Hanhikivi 1 site applied the maximum observed magnitude as such [20] and with an arbitrary increment [7, 8] as the maximum magnitude. In the major project by Saari et al. (2015) [11], a more systematic approach known as the Kijko approach in [21] was introduced to the Hanhikivi 1 site. The method applies confidence levels to a set of given maximum magnitudes based on the seismic catalog and the Gutenberg-Richter relation. In [11], weight factors corresponding to the confidence levels were assigned to maximum magnitude values $m_{\max}$ = 5,5; 6,0; 6,5 and 7,0. The highest evaluated maximum magnitude, $m_{\max}$ = 7,0, was based on Koskinen (2013) [22] and EU-project SHARE (2014) [23].

Selecting the attenuation relationships applicable to the Finnish seismotectonic conditions in step 3 has been a difficult subject in the Hanhikivi 1 PSHA. The PSHAs conducted between 2008 - 2010 applied the Atkinson-Boore, Toro [6, 8] and a Dahle-based GMPE [7]. In response to the abundance of applicable GMPEs, Saari et al. (2015) [11] conducted a literature survey to find the most suitable GMPE based on a list of selection criteria. The survey resulted in the Pezeshk GMPE that was originally designed for eastern North America (NA), an area seismically similar to Fennoscandia. The report also introduces the Fennoscandian GMPE developed by scaling the Pezeshk GMPE with a multiplying function to fit the empirical earthquake data in Fennoscandia. In 2017, VTT concluded that the Fennoscandian GMPE (FGMPE) should not be used in seismic hazard calculations

[13] leading to an update report by Vuorinen (2018) [14]. During the revision of the GMPEs in [14], an error was discovered in the seismic data processing, but the effect on the seismic activity parameters was estimated to be negligible [24] i.e. the parameters in [11] remain valid. The update in the FGMPE lead to corresponding updates in the DBE [15] and DEC C PGA [16]. Subsequently, the GRS were computed for an extensive range of exceedance frequencies (AFE = 10^{-2} - 10^{-9} a^{-1}) and presented along the seismic hazard curve for the PGA [17]. Challenges in the GMPE selection initiated a new project in SAFIR2018 to update the Fennoscandian seismic database and develop a new GMPE for the nuclear industry in Finland. The project resulted in the modified G16 GMPE by Fülöp et al. (2019) [2] derived from the G16 model by Graizer (2016) [25].

Probabilistic assessment requires defining the uncertainty of the aforementioned parameters to assess the confidence. In risk analysis, uncertainties are generally categorized as either aleatory or epistemic. Aleatory uncertainty is the intrinsic randomness of a phenomenom which cannot be reduced with more data, whereas epistemic uncertainty is attributed to the lack of knowledge about the model describing the phenomenom [18]. In the current PSHA [11], uncertainty regarding the seismic activity rate, GR parameter and maximum magnitude is aleatoric. Aleatoric uncertainty taken into account by applying weights to the logic tree branches following the probability distribution of the variable. Uncertainty in the seismotectonic model and GMPE is epistemic and it is considered by including multiple models in the logic tree.

The PSHA results are typically expressed as a ground respose spectrum (GRS) computed by assuming a one-dimensional oscillator at the site and evaluating the logic tree for a given damping factor and a spectrum of natural oscillating frequencies [1]. The seismic hazard calculations evaluated in the logic tree have been carried out by commercial software EZ-FRISK in Saari et al. (2015) [11] and the consecutive reports [15–17]. Although YVL guide B.7 only explicitly requires the GRS to be computed for the DBE frequency (10^{-5} a^{-1}), a range of annual frequencies of exceedance must be considered for seismic probabilitic risk assessment [18]. The last step, taking account of the site response, is ignored since the Hanhikivi 1 plant will be founded directly on bedrock [11].

Chapter 3

Theory

3.1 Magnitude

3.1.1 $m_{\max}$ cumulative distribution function

In 1949, Gutenberg and Richter introduced a relation between the rate and the magnitude of earthquakes [26]. The Gutenberg-Richter relation states that the number of earthquakes generally follows a distribution given by

$$\lg(\lambda_m) = a - bm, \tag{3.1}$$

where λ_m is the rate of earthquakes with a magnitude greater than m, and a and b are constants.

Equation (3.1) can be used to derive the cumulative distribution function (CDF) of magnitude m bounded between $[m_{\min}, m_{\max}]$. The Gutenberg-Richter CDF of m for $m \in [m_{\min}, m_{\max}]$ is given by

$$\begin{aligned} F_M(m) &= \frac{\lambda_{m_{\min}} - \lambda_{\mathrm{m}}}{\lambda_{m_{\min}} - \lambda_{m_{\max}}} \\ &= \frac{1 - 10^{-b(m-m_{min})}}{1 - 10^{-b(m_{max}-m_{min})}}. \end{aligned} \tag{3.2}$$

Equation (3.2) is occasionally presented with exponential base [27]. The CDF of magnitude m with the double-truncated Gutenberg-Richter relation over the entire magnitude range then becomes

$$F_M(m, m_{\max}, m_{\min}) = \begin{cases} 0, & \text{if } m < m_{\min} \\ \dfrac{1 - e^{-\beta(m - m_{\min})}}{1 - e^{-\beta(m_{\max} - m_{\min})}}, & \text{if } m_{\min} \leq m \leq m_{\max} \\ 1, & \text{if } m > m_{\max} \end{cases} \quad (3.3)$$

where $\beta = b\ln(10)$ for b in equation (3.1) is known as the GR parameter. Figure 3.1 shows equation (3.3) plotted as a function of magnitude.

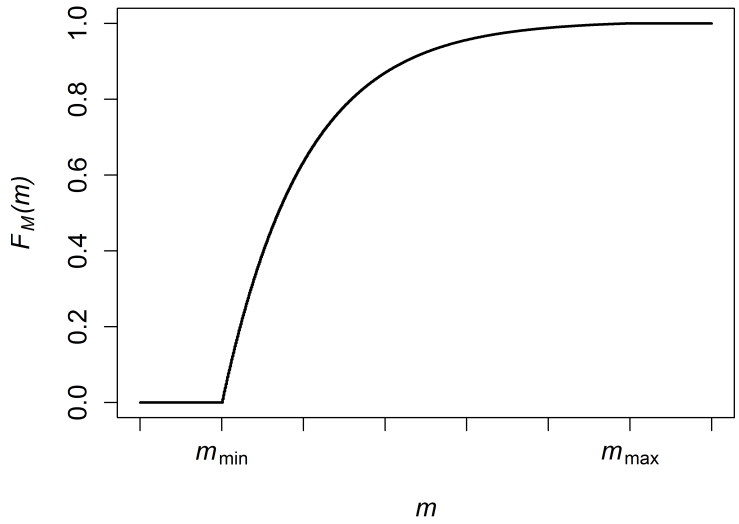

Figure 3.1: Cumulative distribution function of magnitude m in equation 3.3. Maximum and minimum magnitudes represent sharp cut-off magnitudes.

3.1.2 Kijko approach to $m_{\max}$ assessment

Kijko (2004) [27] presented a method to estimate maximum magnitude $m_{\max}$ and standard deviation $\sigma_{m_{\max}}$ from the given seismic catalog. In this work, the seismic events are assumed to follow the double-truncated GR relation, but the method can be applied to any magnitude-frequency relation [27].

Let us assume a catalog of n earthquakes with known minimum magnitude $m_{\min}$ and unknown maximum magnitude $m_{\max}$. The CDF of the maximum observed magnitude $m_{\max}^{\text{obs}}$ is given by [27]

$$F_{M_n}(m_{\max}^{\text{obs}}) = [F_M(m_{\max}^{\text{obs}}, m_{\min}, m_{\max})]^n, \tag{3.4}$$

where $F_M(m, m_{\min}, m_{\max})$ is the CDF in equation (3.3).

The expected value of $m_{\max}^{\text{obs}}$ is [27]

$$\begin{aligned} E(m_{\max}^{\text{obs}}) &= \int_{m_{\min}}^{m_{\max}} m\, dF_{M_n}(m) \\ &= m_{\max} - \int_{m_{\min}}^{m_{\max}} F_{M_n}(m)\, dm. \end{aligned} \tag{3.5}$$

Hence, equation (3.5) can be estimated as

$$m_{\max} \approx m_{\max}^{\text{obs}} + \int_{m_{\min}}^{m_{\max}} F_{M_n}(m)\, dm. \tag{3.6}$$

The integral can be simplified with Cramér's approximation [28]. Equation (3.5) then takes the form

$$m_{\max} = m_{\max}^{\text{obs}} + \frac{E_1(n_2) - E_1(n_1)}{\beta e^{-n_2}} + m_{\min} e^{-n}, \tag{3.7}$$

where $E_1(z)$ is the exponential integral function given by

$$E_1(z) = \int_z^{\infty} \frac{e^{-\zeta}}{\zeta} d\zeta \tag{3.8}$$

that takes parameters $n_1 = n/(1 - \exp(-\beta(m_{\max} - m_{\min})))$ and $n_2 = n_1 \exp(-\beta(m_{\max} - m_{\min}))$.

The variance of $m_{\max}$ is given by

$$\text{Var}(m_{\max}) = \sigma_M^2 + \Big(\frac{E_1(n_2) - E_1(n_1)}{\beta e^{-n_2}} + m_{\min} e^{-n}\Big)^2, \tag{3.9}$$

where σ_M denotes the standard deviation in the determination of $m_{\max}^{\text{obs}}$.

3.1.3 Assessing weights for $m_{\max}$ values

Let us assume the cumulative distribution function in equation (3.4). The probability of that out of n events there will be an earthquake with magnitude $z > m$ is

$$\Pr_{m_{\max},m_{\min}}(z > m) = 1 - F_{M_n}(m^{\text{obs}}_{\max}), \tag{3.10}$$

given that the magnitude distribution is limited by $m_{\max}$ and $m_{\min}$. Equation (3.10) represents the confidence level of $m_{\max}$ when $m^{\text{obs}}_{\max}$ and n are given.

The unnormalized weight for $m_{\max}$ is defined as the limited confidence level given by

$$W_0(m_{\max}) = \Pr_{m_{\max},m_{\min}}(z > m^{\text{obs}}_{\max}) - \Pr_{m_{\max}-\Delta m,m_{\min}}(z > m^{\text{obs}}_{\max}), \tag{3.11}$$

which can regarded as the probability of an earthquake with magnitude $z \in [m^{\text{obs}}_{\max}, m_{\max}]$ for interval $m_{\max} \in [m_{\max} - \Delta m, m_{\max}]$. Typically, the interval between the $m_{\max}$ values is applied as interval Δm. The weight factor determination process is illustrated in figure 3.2.

The final weight factors are normalized, giving us

$$W(m_{\max}) = \frac{W_0(m_{\max})}{\Sigma_{m=\{m_{\max}\}} W_0(m)}. \tag{3.12}$$

3.2 Ground motion prediction

3.2.1 Ground motion

In seismic hazard assessment, the primary interest is the ground motion at the site induced from the source. This section introduces the parameters characterizing ground motion. Here, we only discuss the peak ground acceleration (PGA) and spectral acceleration (SA) as they are applied in Finland [1].

PGA is defined as the maximum amplitude recorded by an accelerogram at one location during a single earthquake. The spectral response is defined by

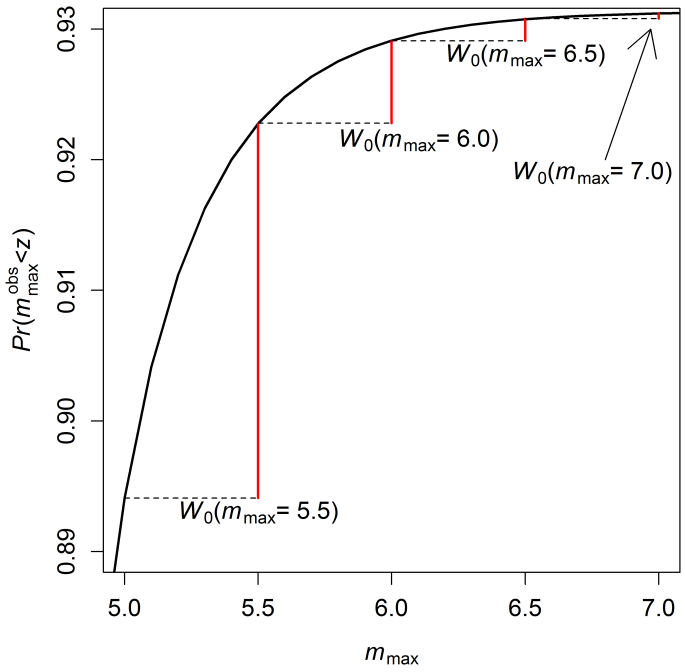

Figure 3.2: Function (3.10) plotted with respect to $m_{\max}$ for $m_{\min} = 1,1$, $m_{\max}^{\text{obs}} = 4,3$ and $n = 11\ 064$. The red lines show the unnormalized weights in equation (3.11) for $\Delta m = 0,5$.

a one-dimensional damped harmonic oscillator at position $x(t)$ subjected to recorded amplitude $a(t)$. The equation of motion of the oscillator is given by [29]

$$\ddot{x}(t) + 2\beta\omega\dot{x}(t) + \omega^2 x(t) = -a(t), \tag{3.13}$$

where β is the damping factor commonly assumed as 0,05 (5% damping) in Finland and ω is the angular frequency defined as $\omega = 2\pi f$, where f is the spectral frequency.

Spectral acceleration is defined as the maximum response felt at the site, i.e.

$$\text{SA}(\beta, \omega) = |\ddot{x}(t) + a(t)|_{\max}. \tag{3.14}$$

SA plotted as a function of f is known as the ground response spectrum (GRS). A GRS describes the maximum response of a harmonic oscillator of varying natural frequency forced into motion by the same vibration. In case of a rigid oscillator, i.e. when $\omega \to 0$, the SA in equation 3.14 becomes

$$\lim_{\omega \to 0} \mathrm{SA}(\beta, \omega) = |a(t)|_{\max}, \tag{3.15}$$

which is equal to PGA.

Ground motion prediction equations (GMPEs) estimate the ground motion at the site region. GMPEs predict the probability distribution of the ground motion rather than a single intensity value to account for the significant variance. GMPEs take the general form

$$\ln Y = \overline{\ln Y(m, r, \theta)} + \epsilon \sigma_{\ln Y}(m, r, \theta), \tag{3.16}$$

where ϵ is a random variable, $\overline{\ln Y(m, r, \theta)}$ and $\sigma_{\ln \mathrm{Y}}(m, r, \theta)$ are the mean and the standard deviation of the ground motion intensity given as a function of magnitude m, distance r and possible other parameters denoted as θ. Random variable ϵ follows the normal distribution with parameters as $\epsilon \propto \mathcal{N}(0, 1)$.

Geometric mean horizontal component is a standard GM parameter provided in many databases [14]. The geometric mean is given by

$$\bar{Y}(\omega) = \Big(\prod_{i=1}^{n} Y_i(\omega) \Big)^{\frac{1}{n}}, \tag{3.17}$$

where ω is the natural angular frequency of the oscillator and $Y_i(\omega)$ is the ground motion for the n considered components. Typically two orthogonal horizontal components are chosen ($n = 2$) and the vertical component is expressed by a separate V/H ratio. In this work, GM is given in geometric mean horizontal component unless otherwise mentioned.

3.2.2 Pezeshk and Fennoscandian GMPEs

Pezeshk et al. (2011) [30] introduced a GMPE for the seismically quiet eastern North America applicable in ranges $R_{\mathrm{hyp}} \in$ [0, 1000 km] and $M_w \in$ [5,0; 8,0]. The GMPE was stochastically adjusted from different empirical GMPEs developed for the more active western North America.

The Pezeshk GMPE is of the form

$$\begin{aligned}\overline{\lg(Y_{\mathrm{PEZ}})} = {} & c_1 + c_2 M_w + c3 M_w^2 + \\ & (c_4 + c_5 M_w) \cdot \min(\lg(R), \lg(70)) + \\ & (c_6 + c_7 M_w) \cdot \max(\min[\lg(R/70), \lg(140/70)], 0) + \\ & (c_8 + c_9 M_w) \cdot \max(\lg(R/140), 0) + \\ & c_{10} R,\end{aligned} \tag{3.18}$$

where R is given by

$$R = \sqrt{R_{\mathrm{rup}}^2 + c_{11}^2}, \tag{3.19}$$

where Y_{PEZ} is the median PGA or SA, M_w is the moment magnitude, R_{rup} is the closest distance to the fault rupture and c_1 - c_{11} are constants.

The mean standard deviation of $\lg(Y_{\mathrm{PEZ}})$ is estimated as [30]

$$\sigma_{\lg(\bar{Y}_{\mathrm{PEZ}})}(M_w) = \begin{cases} c_{12} M_w + c_{13}, & \text{if } M_w \leq 7, \\ -6,95 \cdot 10^{-3} M_w + c_{14}, & \text{if } M_w > 7, \end{cases} \tag{3.20}$$

where c_{12} - c_{14} are constants. Constants c_1 - c_{14} are listed in [30].

The Fennoscandian GMPE (FGMPE) was developed by scaling the Pezesk GMPE in equation 3.18 to the Fennoscandian database compiled in [11] and [14]. The resulting GMPE agrees with the Fennoscandian measurements while maintaining the attenuation behavior of the Pezeshk GMPE. The spectral frequency dependent applicability range of the FGMPE is given in [11].

The Fennoscandian GMPE can be expressed as [14]

$$\lg(Y_{\mathrm{FGMPE}}) = \lg(F) + \lg(Y_{\mathrm{PEZ}}), \tag{3.21}$$

where Y_{PEZ} is the prediction by Pezeshk and F is the multiplying function given by

$$\lg(F) = c_0 + \min(M_w - M_{\mathrm{min}},\, 0) \cdot (c_1 + c_2 \cdot \min(R_{\mathrm{hyp}} - R_1,\, 0)), \tag{3.22}$$

where c_0 - c_4 are the least-squares fitted coefficients, M_w is the moment magnitude, R_{hyp} is the hypocentral distance and R_1 is the first critical reflection distance (70 km in [14]).

The standard deviation of $\lg(Y_{\mathrm{FGMPE}})$ was approximated by the root mean square error (RMSE) given by

$$\sigma_{\lg(Y_{\mathrm{FGMPE}})} = \sqrt{\frac{1}{n}\sum_{i=1}^{n}\Big(\lg(\bar{Y}_i) - \lg(a_i)\Big)^2}, \tag{3.23}$$

where n is the number of measurements, a_i is the empirically measured ground motion acceleration and $\bar{Y}_i$ is the ground motion prediction for a_i. Coefficients c_1 - c_4 and standard deviation values $\sigma_{\lg Y}$ are listed [14].

3.2.3 Modified G16 GMPE

Fülöp et al. (2019) [2] developed a new GMPE to the Fennoscandian conditions applicable in ranges $R_{\mathrm{rup}} \in [0,\ 600\ \mathrm{km}]$ and $M_w \in [2{,}0;\ 7{,}0]$. The modified G16 GMPE is based on the G16 model introduced by Graizer (2016) [25]. The G16 GMPE expresses the ground motion as a series of filters G_n, where each of them represents a physical phenomenom affecting the radiation of seismic waves.

PGA predicted by the modified G16 GMPE is given by [2]

$$\mathrm{PGA}(M_w, R_{\mathrm{rup}}) = G_1(M_w)\cdot G_2(M_w, R_{\mathrm{rup}})\cdot G_3(M_w, R_{\mathrm{rup}})\cdot G_4\cdot C_{\mathrm{mean}}, \tag{3.24}$$

where M_w is the moment magnitude, R_{rup} is the closest distance to the rupture, G_1 - G_4 are the filters for the magnitude scaling, distance attenuation, anelastic attenuation and site correction, respectively, and C_{mean} is the legacy coefficient from converting ground motion measures.

The filters in equation (3.24) are given by

$$G_1(M_w) = (c_1 \cdot \arctan(M_w + c_2) + c_3)\cdot F, \tag{3.25}$$

$$G_2(M_w, R_{\mathrm{rup}}) = \left(\left(1 - \left(\frac{R_{\mathrm{rup}}}{R_{\mathrm{cor}}}\right)^{S_l}\right)^2 + 1,96\cdot D_2^2\cdot\left(\frac{R_{\mathrm{rup}}}{R_{\mathrm{cor}}}\right)^{S_l}\right)^{-1/2}, \tag{3.26}$$

$$G_3(M_w, R_{\mathrm{rup}}) = \exp\Big(-\frac{c_{11} + c_{12}\cdot M_w}{Q_0}\cdot R_{\mathrm{rup}}\Big) \tag{3.27}$$

and

$$G_4 = 0,575, \tag{3.28}$$

where the distance correction factor is defined as $R_{\text{cor}} = c_4 + M_w \cdot c_5$, the magnitude dependent slope factor is $S_l = \epsilon_1 M_w + \epsilon_2$, and c_n, F, D_2, Q_0 and ϵ_n are constants listed in [2]. The site correction filter assumes a constant $v_{s30} = 2\ 800$ m/s, which is a common approximation in Fennoscandia [2].

In the modified G16 model, the SA is obtained by scaling the PGA with normalization factor SA_{norm}. The SA at period $T = f^{-1}$ is thus given by

$$\text{SA}(T, M_w, R_{\text{rup}}) = \text{PGA}(M_w, R_{\text{rup}}) \cdot \text{SA}_{\text{norm}}(T, M_w, R_{\text{rup}}). \tag{3.29}$$

The normalization factor in equation (3.29) is defined as

$$\begin{aligned} \text{SA}_{\text{norm}}(T, M_w, R_{\text{rup}}) = I \cdot \exp\Big(-0,5\Big(\frac{\ln(T) - \mu}{S}\Big)^2\Big) \\ + \Big(\Big(1 - \Big(\frac{T}{T_{sp,0}}\Big)^{\zeta}\Big)^2 + 4D_{sp}^2\Big(\frac{T}{T_{sp,0}}\Big)^{\zeta}\Big)^{-1/2}, \end{aligned} \tag{3.30}$$

where $T_{sp,0}$ and μ are the factors controlling the peak amplification frequency, S controls the width of the spectra and constants I and ζ (given in [2]) control the spectral amplification and slope, respectively.

The peak amplification frequency and spectral width factors in equation (3.30) are defined as

$$\mu = m_1 R_{\text{rup}} + m_2 M_w + m_3, \tag{3.31}$$

$$T_{sp,0} = \max(t_1 R_{\text{rup}} + t_2 M_w + t_3, 2e^{-\mu}), \tag{3.32}$$

and

$$S = s_1 \cdot R_{\text{rup}} - (s_2 \cdot M_w + s_3), \tag{3.33}$$

where constants m_n, t_n and s_n are listed in [2].

3.2.4 Modified Dahle GMPE

Dahle et al. (1990) introduced a GMPE for the Northwestern Europe. The GMPE was calibrated with a database comprising intraplate measurements from several continents.

Let us assume the ground motion amplitude to be of the form [3]

$$Y = \frac{Y_0}{R_{\text{hyp}}^b} e^{aM + qR_{\text{hyp}}}, \tag{3.34}$$

where R_{hyp} denotes hypocentral distance, M denotes magnitude and Y_0, a, b and q are constants.

The logarithm of equation (3.34) then becomes

$$\ln(Y) = \ln(Y_0) + aM - b\ln(R_{\text{hyp}}) + qR_{\text{hyp}}. \tag{3.35}$$

Distance-dependence of the geometric spreading is assumed to be of the form [3]

$$G(R_{\text{hyp}}, R_0) = \begin{cases} R_{\text{hyp}}^{-1}, & \text{if } R_{\text{hyp}} \leq R_0, \quad \text{(3.36a)} \\ R_0^{-1}\left(\frac{R_0}{R_{\text{hyp}}}\right)^{5/6}, & \text{if } R_{\text{hyp}} > R_0, \quad \text{(3.36b)} \end{cases}$$

where R_0 is the hypocentral distance where the spherical spreading of S waves is overtaken by the cylindrical spreading of Lg waves [3]. The recommended value is $R_0 = 100$ km [3, 7].

Substituting equations (3.36a) - (3.36b) in equation (3.35) and renaming constants then gives us

$$\ln(Y) = c_1 + c_2 M + c_3 \ln G(R, R_0) + c_4 R, \tag{3.37}$$

where c_1 - c_4 are the coefficients to be determined. The optimized Dahle GMPE is shown in figure 3.3.

The Dahle GMPE predicts the ground motion to fall log-log-linearly with respect to distance in the range of $R_{\text{hyp}} \leq 10$ km, as shown in figure 3.3. Dahle et al. (1990) [3] assumes earthquakes to be point-sourced, while fault

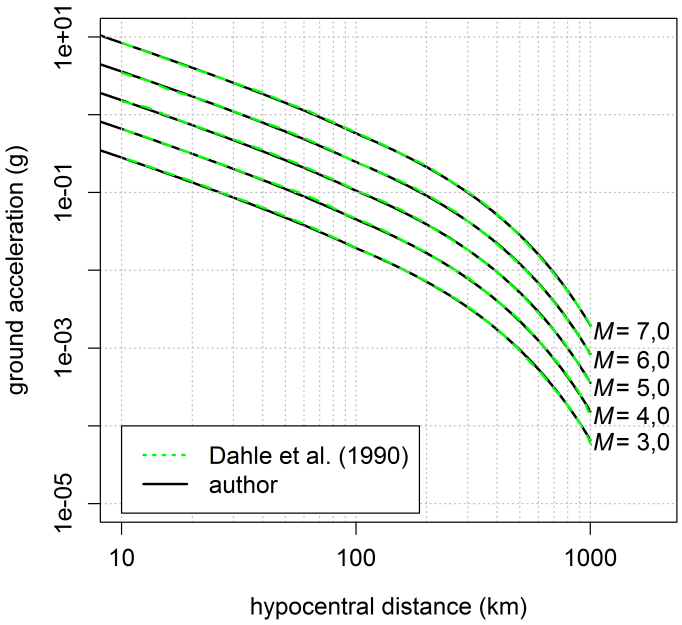

Figure 3.3: PGA at different magnitudes predicted by Dahle et al. (2990) [3]. The coefficients are $c_1 = -1,471$, $c_2 = 0,849$, $c_3 = 1,0$ and $c_4 = -0,00418$. The solid line shows the verification of our GMPE computation.

widths at the Hanhikivi site are shown to exceed even one kilometer for $M_w \geq 4,0$ [31]. Therefore, the attenuation gradient is unrealistic in near distances at large magnitudes. This conclusion is further supported by a prior report [8], where the Atkinson-Boore GMPE was excluded from PSHA based on its log-log-linear attenuation.

One possibility to resolve the contradiction is by assuming a constant attenuation in near-distance. Applying this assumption for $R_{\text{hyp}} \leq 10$ km gives us the modified Dahle function

$$\ln Y = \begin{cases} c_1 + c_2 M - c_3 R_c + c_4 R_c, & \text{if } R_{\text{hyp}} \leq R_c, \quad (3.38a) \\ c_1 + c_2 M - c_3 \ln(R_{\text{hyp}}) + c_4 R_{\text{hyp}}, & \text{if } R_c \leq R_{\text{hyp}} \leq R_0, \quad (3.38b) \\ c_1 + c_2 M - c_3 \ln(R_0^{1/6} R_{\text{hyp}}^{5/6}) + c_4 R_{\text{hyp}}, & \text{if } R_{\text{hyp}} > R_0, \quad (3.38c) \end{cases}$$

where $R_c = 10$ km.

3.3 Seismic hazard analysis

The ability to predict ground motion is a key element of seismic hazard analysis. As stated in equation (3.16), ground motion y follows distribution $\ln(y) \propto \mathcal{N}(\overline{\ln(Y)}, \sigma^2_{\ln(Y)})$. The probability of exceeding ground motion intensity y then becomes

$$P(Y > y|m, r) = 1 - \Phi\Big(\frac{\ln(y) - \overline{\ln Y(m, r)}}{\sigma_{\ln(Y)}}\Big), \tag{3.39}$$

where $\Phi(x)$ is the CDF of normal distribution.

The overall probability of an earthquake with an intensity above y occurring can be expressed as [32]

$$P(Y > y) = \int_{m_{\min}}^{m_{\max}} \int_{0}^{r_{\max}} P(Y > y|m, r) f_{M,R}(m, r) dr dm, \tag{3.40}$$

where $f_{M,R}(m, r)$ is the probability distribution of magnitude m and distance r integrated over ranges $[m_{\min}, m_{\max}]$ and $[0, r_{\max}]$, respectively.

Seismic source areas in EZ-FRISK are defined as polygons in the horizontal plane. In EZ-FRISK, the probability in equation (3.40) for source area j becomes [33]

$$P_j(Y > y) = \int_{\rho} \frac{\text{arc}_j(\rho)}{\text{area}_j} \Big(\int_{m} P(Y > y|m) f_{M_j}(m) dm \Big) d\rho, \tag{3.41}$$

where f_{M_j} is the magnitude distribution in source area j, ρ is the horizontal distance from the site, $\text{arc}(\rho)$ is the length of the arc with distance ρ from the source and area_j is the horizontal area of the source calculated as [33]

$$\text{area}_j = \int_{\rho} \text{arc}_j(\rho) d\rho. \tag{3.42}$$

Seismic activity rate and magnitude distribution are constant inside a seismic source area. As a result, the rate of ground motions exceeding amplitude y is given by [32, 33]

$$\lambda(Y > y) = \sum_{j}^{n_{\text{sources}}} \lambda_j \int_{\rho} \frac{\text{arc}_j(\rho)}{\text{area}_j} \Big(\int_{m} P(Y > y|m) f_{M_j}(m) dm \Big) d\rho, \qquad (3.43)$$

where λ_j is the seismic activity rate in source j.

In practice, EZ-FRISK solves for the amplitude with a given time frequency by calculating the activity rates for a list of amplitudes (a_1, a_2, ... , a_n) and earthquake periods (T_1, T_2, ..., T_m), where $T = f^{-1}$ and compiling a matrix as shown below.

	a_1	a_2	...	a_n
T_1	$\lambda(a_1, T_1)$	$\lambda(a_2, T_1)$	...	$\lambda(a_n, T_1)$
T_2	$\lambda(a_1, T_2)$	$\lambda(a_2, T_2)$	...	$\lambda(a_n, T_2)$
...			$\lambda(a_i, T_j)$	
T_m				$\lambda(a_n, T_m)$

Based on the matrix, EZ-FRISK interpolates the amplitude between the activity rates bracketing the targeted AFE.

Chapter 4

Methods

4.1 Fitting of the Dahle function

In this section, we derive a new GMPE based on the Dahle function in equations (3.38a)-(3.38c). The modified Dahle function was calibrated with the following data sets:

1. Fennoscandian earthquake recordings [14],
2. Next Generation Attenuation Relationships for Central & Eastern North-America (NGA-East) [34] and
3. Canadian recordings from Engineering Seismology Toolbox (EST) [35].

The Fennoscandian database was originally compiled by Saari et al. (2015) [11], corrected by Vuorinen et al. (2018) [14] and further updated with recent recordings. We received the database from T. Vuorinen via email. Measurements from CENA (NGA-East and EST) were included to supplement the Fennoscandian data set with high-magnitude data from similar tectonic settings [14]. The database was filtered to only include recordings measured in the hard rock conditions with $v_{s30} \geq 2000$ ms^{-1} and sampling frequency $f_s \geq 100$ Hz. Observed amplitudes can be considered reliable at frequencies below $f_{\text{obs}} = 40$ Hz. The upper limit is based on the engineer's version of Nyquist-Shannon theorem ($f_{\text{obs}} \leq f_{\text{s}}/2,5$) [36]. The limit describes the highest frequency when the signal can be reconstructed without aliasing effects while considering the inaccuracy attributed to measuring. It should be noted that the GM intensity in NGA-East is given in median rotated component (RotD50), but here, it is used interechangeably with the geometric mean [14].

In addition to choosing the database sources, consideration must be given to the magnitude and distance ranges of the database. The main challenge is in avoiding letting non-damaging microearthquakes control the calibration while retaining a sufficient amount of calibration data. We base our definition of the safety-significant magnitude and distance ranges on the deaggregation study in [11], where the mean (M_w, R_{hyp}) for PGA = 0,2 g and 0,02 g were (2,4; 6,9 km) and (2,3; 20 km), respectively. Majority of the measurements are insignificant to nuclear safety, as shown in figure 4.1. We filtered out events below magnitude $M_w = 2,0$ based on the deaggregation study and the cut-off magnitude in Fülöp et al. (2019) [2]. Cut-off distance $R_{\text{hyp}} = 150$ km was selected, as we aimed to retain about the same number of measurements below and above $R_{\text{hyp}} = 100$ km, where the method of the geometric spreading in equations (3.36a) - (3.36b) changes. The modified Dahle function has relatively few coefficients to fit, compared to e.g. [2], allowing a calibration with fewer measurements and, consequently, the relatively low cut-off distance. A summary of the filtered database is given in table 4.1 while figure 4.2 shows its magnitude and distance distribution.

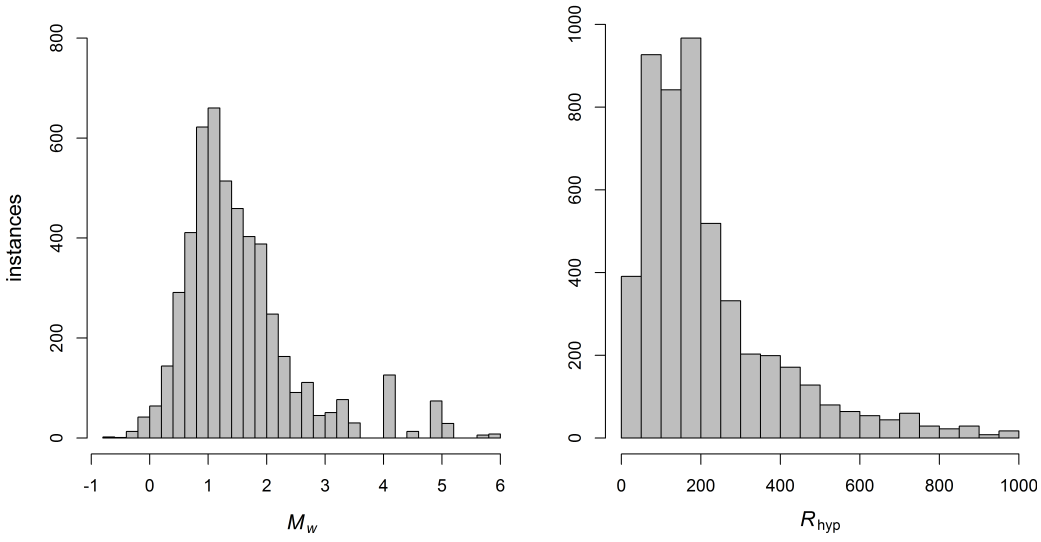

Figure 4.1: Histograms of the seismic database distributed by moment magnitude (left) and hypocentral distance (right) before filtering by magnitude and distance.

We wrote a C++ program to optimize the modified Dahle function in equations (3.38a) - (3.38c). The program was designed to loop through a range of coefficients $c_1 - c_4$ and return the set of coefficients giving the minimum

Table 4.1: Summary of the seismic data used to calibrate the modified Dahle GMPE.

	Fennoscandia	CENA
Number of recording stations	57	11
Epicentral distance range (km)	4,87 - 149	22,4 - 146
Depth range (km)	1,0 - 36,9	16,4 - 26,0
Moment magnitude range	2,0 - 4,5	5,0 - 5,9
Number of events	78	3
Number of measurements	198	11

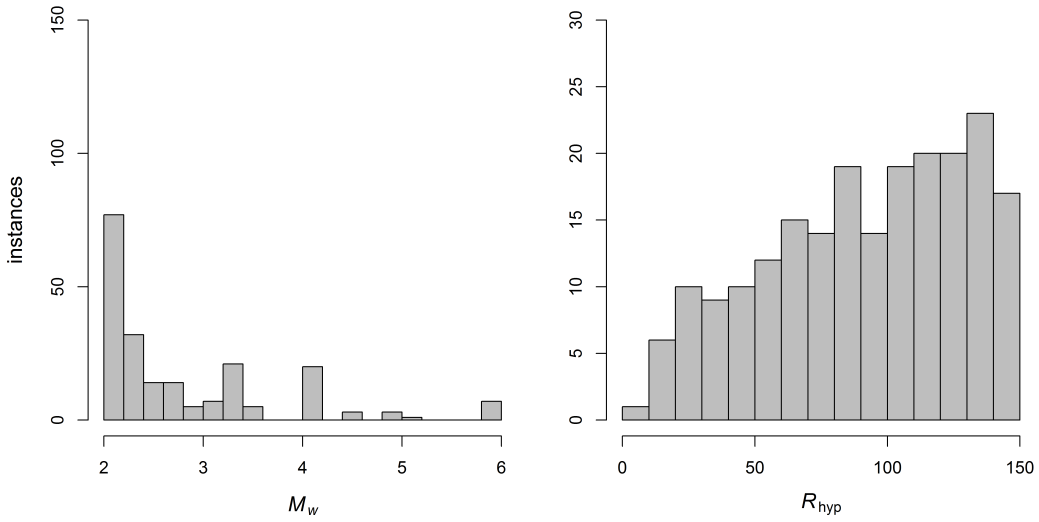

Figure 4.2: Histograms of the calibration data for the modified Dahle GMPE distributed by moment magnitude M_w (left) and hypocentral distance R_{hyp} (right).

RMSE (see equation (3.23)) for the filtered database in table 4.1. The computationally heavy optimization was parallelized with a BASH script and performed on a computing cluster. The process was repeated for every spectral frequency and the resulting optimized parameters are listed in table 4.2. While our optimized $\sigma_{\lg(Y)}$ values are high ($\sigma_{\lg(Y)} > 0{,}35$), they are still considered acceptable ($\sigma_{\lg(Y)} < 0{,}55$) [37]. Figure 4.3 shows the modified Dahle GMPE fitted for the PGA. Figures of the fits at other spectral frequencies are presented in appendix A. These figures show that on the mean level, the ground motion is not nuclear safety significant (GM $\geq$ 0,1 g) below $M_w =$ 5,0. Figure 4.4 shows the residual of the fit (res $= \lg(\text{GM}_{\text{Dahle}}) - \lg(\text{GM}_{\text{obs}})$)

distributed by magnitude M_w and distance R_{hyp}. The residual appears evenly distributed by magnitude, but the distribution by distance deviates. To examine the deviation, we calculated the average shift in distance $R_{\text{hyp}} \leq R_0$ defined as

$$\text{shift} = \Big(\sum_{i=1}^{n} w_{R_0}(R_{\text{hyp},i}) \Big)^{-1} \sum_{i=1}^{n} \Big(w_{R_0}(R_{\text{hyp},i})(\lg(\bar{Y}_i) - \lg(a_i)) \Big), \qquad (4.1)$$

where n is the number of measurements, a_i is the empirically measured ground motion acceleration, $R_{\text{hyp},i}$ is the hypocentral distance of a_i, $\bar{Y}_i$ is the ground motion prediction for a_i and $w_{R_0}(R_{\text{hyp},i})$ is the weight factor equaling one when $R_{\text{hyp},i} \leq R_0$ and zero elsewhere.

The shifts calculated for $R_0 = 30$ and 50 km are presented in table 4.3. A systematic shift can be observed in table 4.3 but the shifts are insignificant compared to other uncertainties related to the derivation of GMPEs. For example, the maximum shift of 0,139 in table 4.3 merely corresponds to a relative difference of 38%. The shift in range $R_{\text{hyp}} \leq 10$ km is significantly large, exceeding 1,0 at every spectral frequency. Unfortunately, there is only one measurement of magnitude $M_w = 2,2$ in this range so we cannot make conclusions on the reliability of the fit below $R_{\text{hyp}} = 10$ km.

Table 4.2: Optimized coefficients of the optimized Dahle GMPE in equations (3.38a)-(3.38c). Coefficient c_3 was restricted to be non-negative. Standard deviation $\sigma_{\lg(Y)}$ is equal to the minimized RMSE.

frequency (Hz)	c_1	c_2	c_3	c_4	$\sigma_{\lg(Y)}$	$\sigma_{\ln(Y)}$
PGA	-12,6	2,04	0,075	-0,0210	0,393	0,905
40	-11,2	1,93	0,082	-0,0257	0,434	0,999
33,33	-11,4	1,93	0,059	-0,0229	0,426	0,981
25	-11,7	1,95	0,038	-0,0197	0,418	0,962
20	-12,1	1,99	0,039	-0,0168	0,406	0,935
10	-13,9	2,20	0,049	-0,00873	0,388	0,893
6,67	-15,3	2,43	0,065	-0,00712	0,402	0,926
5	-16,2	2,51	0,053	-0,00599	0,406	0,935
2,5	-18,3	2,75	0,052	-0,00579	0,411	0,946
1	-19,4	2,66	0,077	-0,00945	0,402	0,926
0,5	-19,0	2,31	0,126	-0,0104	0,363	0,836

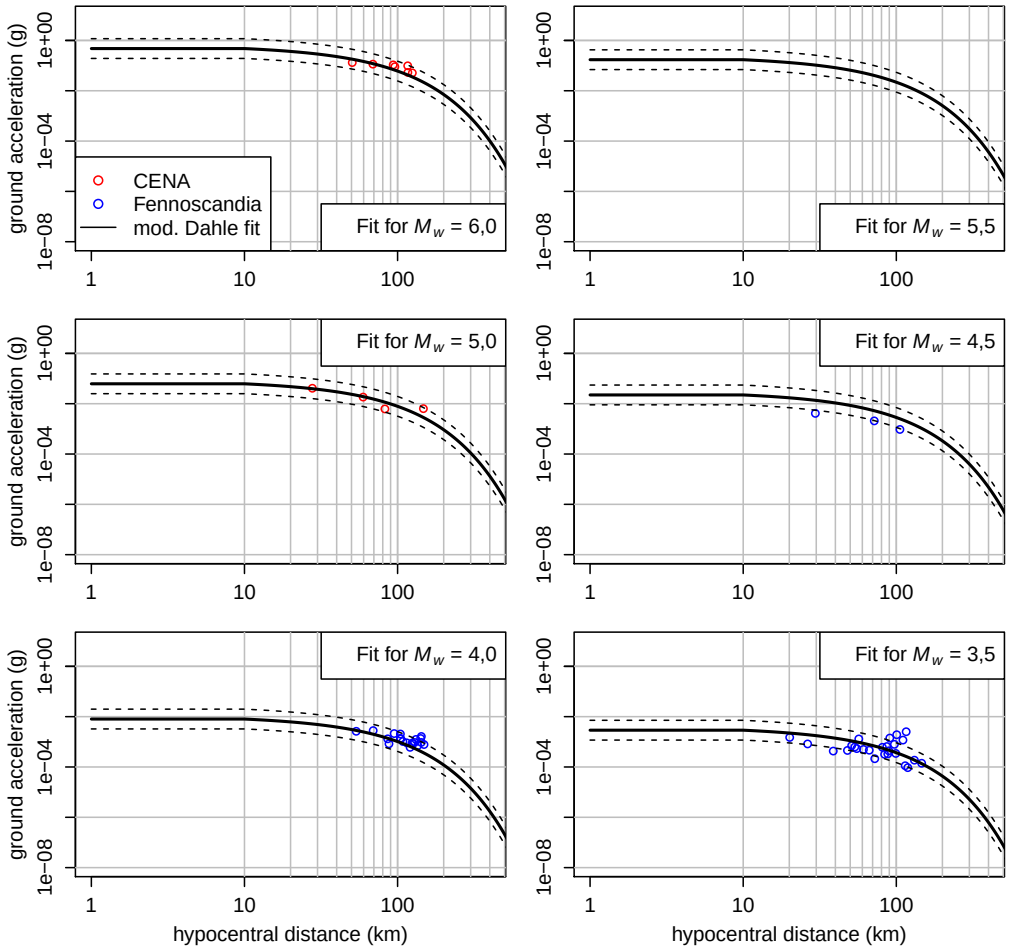

Figure 4.3: The fitted modified Dahle GMPE plotted for the PGA for magnitudes $M_w = 3{,}5$ - $6{,}0$. Dashed lines present the $\overline{\lg(Y)} \pm \sigma_{\lg(Y)}$ errors. The subfigures include data points in the interval $[M_w - \Delta m,\ M_w + \Delta m]$, where $\Delta m = 0,25$.

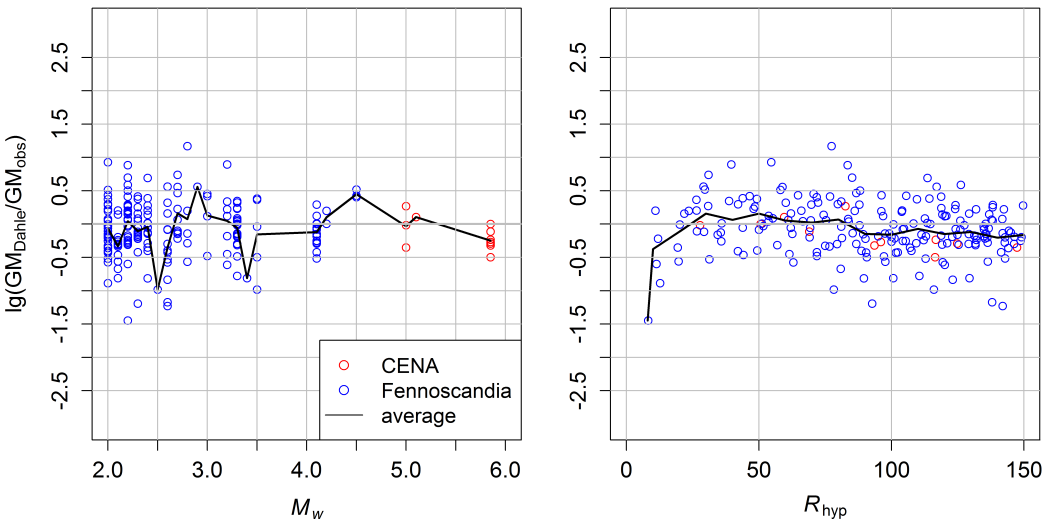

Figure 4.4: Deviation of the modified Dahle function from the calibration data for PGA as a function of moment magnitude (left) and hypocentral distance (right). The solid line shows the average deviation.

Table 4.3: Shifts in close distance to the site calculated with equation (4.1). The modified Dahle GMPE overestimates when the shift is positive and underestimates for a negative shift. The shift approaches zero for a growing R_0.

f (Hz)	$R_0 = 50$ km	$R_0 = 30$ km
PGA	-0,00698	-0,124
40	-0,0180	-0,115
33,33	-0,0201	-0,139
25	0,0127	-0,0690
20	0,0197	-0,0759
10	0,0413	-0,0854
6,67	0,0517	-0,0676
5	0,0665	-0,0875
2,5	0,0571	-0,0958
1	0,0416	-0,104
0,5	0,0244	-0,127

4.2 Comparison of the GMPEs

In this section, we plotted the GMPEs introduced in section 3.2 as a function of distance at different magnitudes to study their behavior. Figures 4.5 - 4.6 show the GMPE comparison for the PGA, while figures at the spectral frequencies are shown in appendix B.

Between range R_{hyp} = 10 - 100 km, the amount of calibration data is sufficient and the GMPEs appear consistent. Although deviations up to around a magnitude in the ground acceleration can be observed, they reflect the general variability in the calibration data. Measurements show differences up to a magnitude in ground acceleration for close moment magnitudes and distances (see e.g. figure 4.3 or figure 4.1 in [14]). Between R_{hyp} = 70 - 140 km, we can observe a discontinuity in the Pezeshk and the Pezeshk-based Fennoscandian GMPE. This feature, arising from the Mohorovičić discontinuity [30], is not seen in the modified Dahle and G16 GMPEs. It is impossible to conclude definitely whether the discontinuity in the ground motion exists solely based on our data. Above R_{hyp} = 200 km all the GMPEs except for the modified Dahle GMPE keep predicting consistent values. This is expected, since the GMPE is not calibrated beyond R_{hyp} = 150 km, as explained in section 4.1.

Predicting ground motion in range R_{hyp} = 1 - 10 km is a challenging task, since the range contributes significantly to the total hazard [11], while the calibration data is scarce. The GMPEs in R_{hyp} = 1 - 10 km start to deviate for a decreasing magnitude. In particular, the modified Dahle GMPE significantly deviates from other GMPEs with the deviation exceeding around a magnitude for $M_w < 5{,}0$ (see figure 4.5 and appendix B). The growing deviation can be understood by comparing the GMPE behavior for a changing magnitude in figure 4.7. The Pezeshk and the Fennoscandian GMPEs appear to converge for an increasing magnitude, while the increment in the modified G16 and Dahle GMPEs is nearly linear. The increment in the modified Dahle GMPE is particularly large leading to the aforementioned deviation in the lower magnitude range. The studied GMPEs show a low attenuation gradient between R_{hyp} = 1 - 10 km, when compared to e.g. the original Dahle function in figure 3.3 or the Atkinson-Boore [8, 38]. The modern GMPEs successfully account for the size of the the fault width discussed in section 3.2.4.

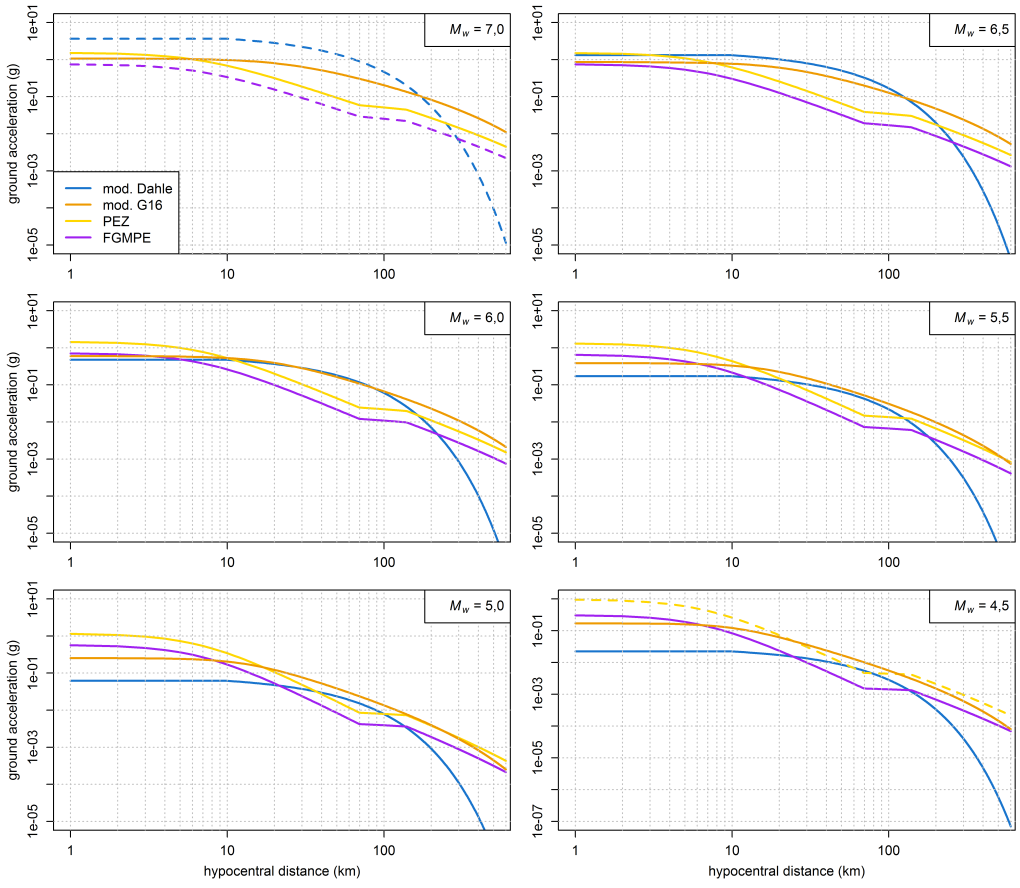

Figure 4.5: The GMPEs plotted for the PGA as a function of hypocentral distance between $M_w = 4{,}5$ - 7,0. Dashed line implies that the GMPE is out of its range of applicability.

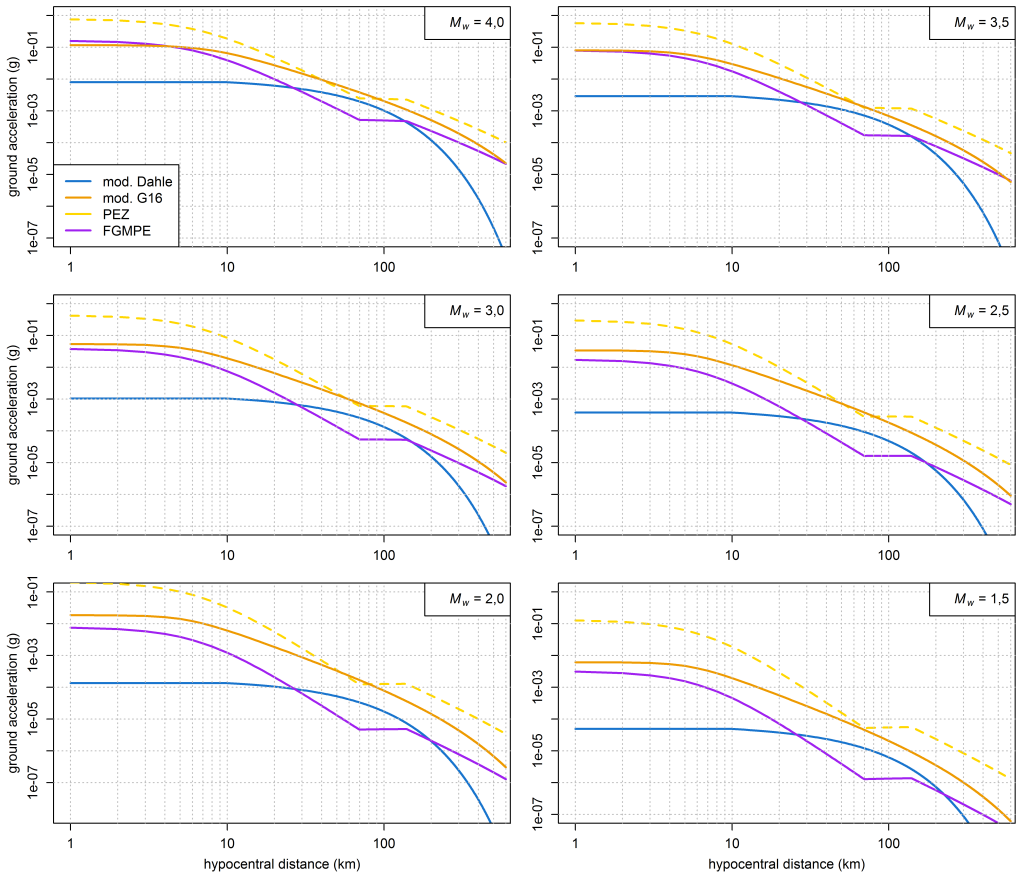

Figure 4.6: The GMPEs plotted for the PGA as a function of hypocentral distance between M_w = 1,5 - 4,0. Dashed line implies that the GMPE is out of its range of applicability.

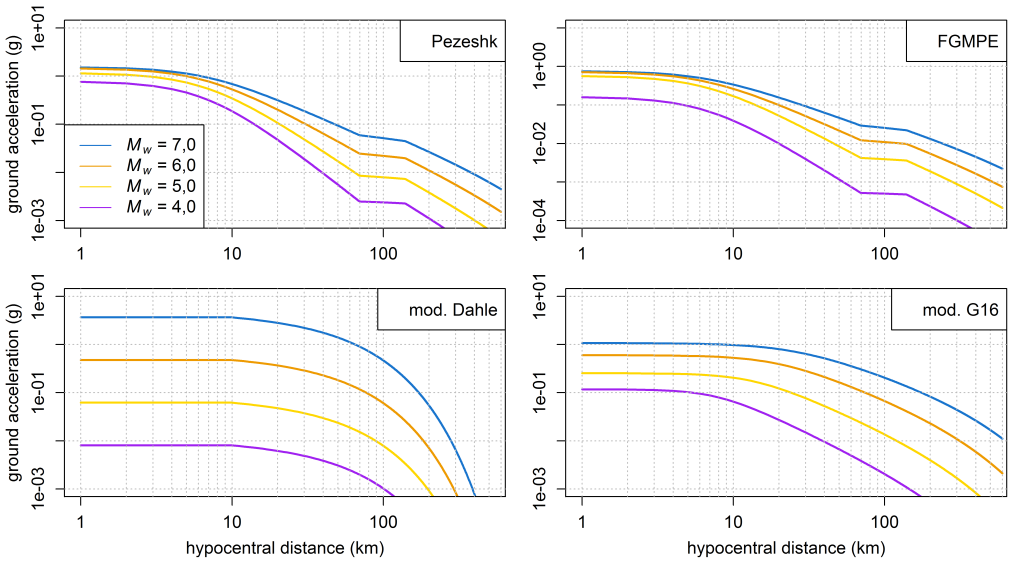

Figure 4.7: The GMPEs plotted for the PGA as a function of hypocentral distance between M_w = 4,0 - 7,0. The purpose of the plots is to illustrate the different trends of convergence below $R_{\text{hyp}} = 10$ km.

4.3 Logic tree

As mentioned in chapter 2, the Hanhikivi 1 PSHA accounts for the uncertainties in the seismotectonic model, seismic parameters λ and β, maximum magnitude $m_{\max}$ and GMPE by evaluating them in a logic tree. The logic tree applied in this work is presented in figure 4.8. We applied the two seismotectonic models presented in [11] with equal weights. Seismic parameres λ and β are assumed to be normally distributed [11]. Normal distribution is symmetric about its mean with 68 % of the distribution in range $[\mu - \sigma, \mu + \sigma]$. Based on this, Saari et al. (2015) [11] selected weights $W(\mu) = 0,68$ and $W(\mu \pm \sigma) = 0,16$. The seismic parameters and their standard deviations are listed in [12].

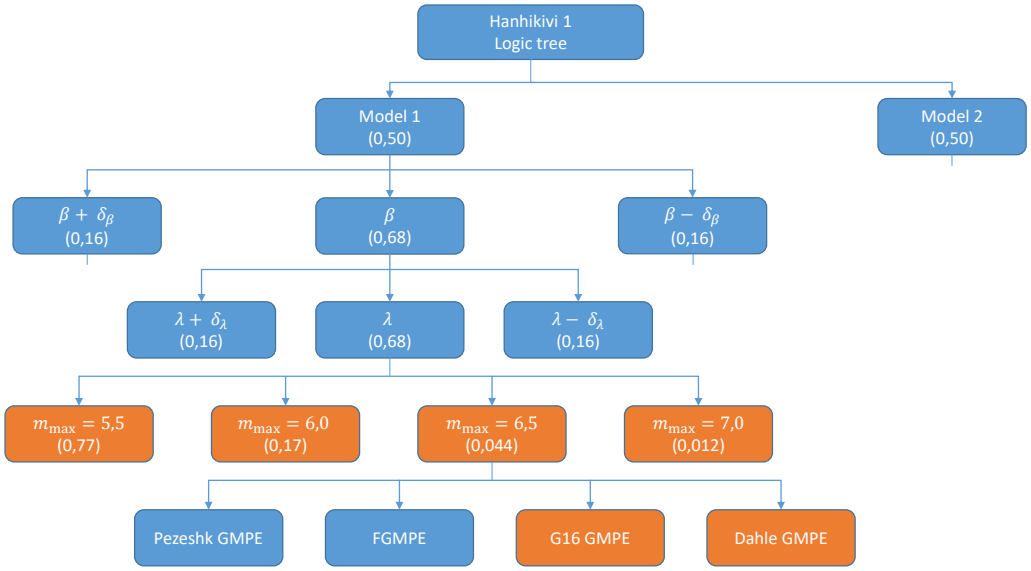

Figure 4.8: Schematic presentation of the logic tree structure used to evaluate the seismic hazard. The orange background color denotes that the node is modified from [11]. The weight of each node, except for the GMPEs, is given in the brackets. The total number of leaf nodes in the thesis is 288.

The current approach to assess the weights for $m_{\max}$ (see section 3.1.3) requires selecting a set of maximum magnitudes. Saari et al. (2015) [11] applied $m_{\max} = \{5,5;\ 6,0;\ 6,5;\ 7,0\}$ with an interval of $\Delta m = 0,5$. The parameters defining the Gutenberg-Richter relation in equation 3.4 were $m_{\min} = 1,1$, $b = 1,1$ and $m_{\max}^{\text{obs}} = 4,3$. The number of earthquakes was calculated as $n = \lambda T$, where λ was 84,5 events/year for the given $m_{\min}$ during

observed time period $T = 131$ years. We repeated the weight assessment in [11], but obtained slightly different values, as shown in table 4.4. The weights calculated here are applied in the logic tree, but the effect of the change on the seismic hazard assessment is expected to be negligible. We attempted to include $m_{\max} = 5{,}0$ in the set of maximum magnitude values, as shown in table 4.4. Resulting weight $W(m_{\max} = 5,0) = 0,86$ was deemed too high considering the current weight distribution and the prior studies on $m_{\max}$ in Fennoscandia (see chapter 4.2 in [11]). Our attempt to extend the magnitude range demonstrates a significant problem in the current method of weight assessment; the method is very sensitive to the lowest $m_{\max}$ value chosen. Following the shortcomings in the current weight assessment method, we attempted to approach the problem by assuming $m_{\max}$ to be normally distributed allowing us to apply the weight distribution of the seismic parameters. We calculated the $m_{\max}$ and $\mathrm{Var}(m_{\max})$ following equations (3.7) - (3.9) with the input parameters in this paragraph. A binary search code was written in R to iteratively solve for $m_{\max}$ in equation (3.7). The exact value of σ_M in equation (3.9) is not known, so we assigned $\sigma_M = 0{,}50$ based the estimate in [20]. The described approach resulted in $m_{\max} = 4,43 \pm 0,51$, which was deemed unreasonably low and rejected. The method, originally applied for the seismically active western NA, likely fails when applied to a seismically less active area. In active areas, the difference between the maximum possible and the maximum observed earthquake can be small, but in less active areas the the maximum earthquake can be significantly stronger than the strongest earthquake in the measurement history.

Table 4.4: The weight distribution of $m_{\max}$ introduced in Saari et al. (2015) [11], calculated in this work with the parameters in [11] and calculated including $m_{\max} = 5{,}0$.

m_{max}	Saari	calculated	extended
5,0	-	-	0,86
5,5	0,70	0,77	0,11
6,0	0,22	0,17	0,024
6,5	0,06	0,044	0,0061
7,0	0,02	0,012	0,0016

In this work, we attempt to include two new GMPEs in the current Hanhikivi 1 PSHA. The GMPE weight distribution applied in the current Hanhikivi 1 PSHA [11] is presented in table 4.5. In section 4.1, it was shown that the modified Dahle function appears to underestimate ground motion near the site ($R_{\mathrm{hyp}} \leq 30$ km). In section 4.2, the modified Dahle function was

shown to predict lower GM estimates near the site when compared to the other GMPEs at low magnitudes. Based on these observations, the Dahle function was given a lower weight than the G16 function. The selected weight ratio between the Dahle and the G16 GMPEs is shown in table 4.6. The upper limit of the magnitude range was estimated as $M_w = 6,5$ based on the magnitude range of FGMPE calibrated with a similar dataset. There is inherent arbitrariness in the selected weight ratios in tables 4.5 - 4.6 as there is no standard process to evaluate the epistemic uncertainty of the GMPEs. A weight ratio of 1:1 was selected between the GMPEs in the current PSHA and the newly introduced GMPEs. Combining tables 4.5 - 4.6 with the selected ratio gives us the total weight distribution shown in table 4.7.

Table 4.5: Weight ratio between the Fennoscandian and the Pezeshk GMPE [11]. The dependence on magnitude and frequency arises from the differing magnitude ranges of applicability and the disagreement between the FGMPE predictions and the empirical data at low spectral frequencies.

$m_{\max}$	$f > 10$ Hz and PGA	$f = 10$ Hz	$f < 10$ Hz
5,5	0,9/0,1	0,9/0,1	0/1
6,0	0,6/0,4	0,6/0,4	0/1
6,5	0,3/0,7	0/1	0/1
7,0	0/1	0/1	0/1

Table 4.6: Weight ratio between the modified G16 and the modified Dahle GMPE.

$m_{\max}$	$\forall f$
5,5 - 6,5	0,7/0,3
7,0	1/0

Table 4.7: Weight ratio between the Fennoscandian, Pezeshk, modified G16 and modified Dahle GMPEs, respectively.

$m_{\max}$	$f > 20$ Hz and PGA	10 Hz	$f < 10$ Hz
5,5	0,45/0,05/0,35/0,15	0,45/0,05/0,35/0,15	0/0,5/0,35/0,15
6,0	0,3/0,2/0,35/0,15	0,3/0,2/0,35/0,15	0/0,5/0,35/0,15
6,5	0,15/0,35/0,35/0,15	0/0,5/0,35/0,15	0/0,5/0,35/0,15
7,0	0/0,5/0,5/0	0/0,5/0,5/0	0/0,5/0,5/0

4.4 Probabilistic seismic hazard assessment

The seismic hazard analyses were computed with EZ-FRISK 7.65 Build 004. Each branch in the logic tree (see figure 4.8) corresponded to a single combination of input parameters. A seismic hazard analysis was performed for each combination, amounting to a total of 288 analyses. We computed the site response for the PGA and a range of spectral frequencies between f = 0,5 and 40 Hz at five annual frequencies of exceedance (AFE = 10^{-4} a^{-1} - 10^{-8} a^{-1}). The spectral frequency range was chosen to include the ranges in prior reports [11, 15]. In addition, we selected the geometric mean horizontal component of spectral response at 5% damping as the intensity measure and 64,53 °N 24,26 °E as the site location. The calculational parameters given to the software are listed in table 4.8. Site parameters, including the v_{s30}, were disregarded as the Hanhikivi site is located on exposed bedrock [11]. A focal depth of d = 45 km was selected since it was used in the prior reports [11, 15, 17]. We applied the attenuation table format in EZ-FRISK to define the GMPEs. The attenuation table records the GM prediction and its deviation as a function of moment magnitude and distance to rupture (Pezeshk, G16) or to the center of energy (FGMPE, Dahle). The distances ranged from 1 to 1000 km (Pezeshk, FGMPE), 600 km (G16) and 200 km (Dahle) with an interval of 5 km, while the moment magnitudes ranged from 0 to 7,0 with an interval of 0,1. We only carried out the seismic hazard analyses with the modified G16 and Dahle GMPEs in this work, since the analyses with the Pezeshk and the Fennoscandian GMPEs were already computed in relation to prior work [17]. The computation process in [17] was verified by comparing to the results by Malm & Kaisko (2017) [15].

The analyses on EZ-FRISK were run manually and the resulting probabilistic spectra (psp) files were saved. A C++ program was written to process the saved files, since it would be prohibitely time-consuming to manually handle the produced data. The program extracted the spectral response values in the psp files and sorted them by AFE and spectral frequency. The sorted data was imported to Excel, where the weight accumulation as a function of acceleration was computed for every time and spectral frequency following the logic tree. Spectral acceleration values were then extracted at different fractiles of the weight accumulation and compiled into ground response spectra (GRS). GRS at varying fractiles are included to display epistemic uncertainty. Fractile levels 5, 15, 50, 85 and 95% were chosen based on convention [11, 18]. Although the assessment on Excel is time-consuming, the visual illustrativeness allows for a better transparency.

Table 4.8: Computational parameters submitted to EZ-FRISK.

Fault sources	
Maximum inclusion distance	1000 km
Down dip integration increment	1 km
Horizontal integration increment	1 km
Number of rupture lengths per earthquake	1
Near source effects	none
Subduction interface sources	
Maximum inclusion distance	1000 km
Down dip integration increment	5 km
Horizontal integration increment	5 km
Number of rupture lengths per earthquake	1
Subduction slab sources	
Maximum inclusion distance	1000 km
Down dip integration increment	5 km
Horizontal integration increment	20 km
Number of rupture lengths per earthquake	1
Area sources	
Maximum inclusion distance	200 km
Default number of rupture azimuths	10
Maximum distance for default azimuths	20 km
Maximum distance for one azimuth	70 km
Use binned calculations if possible	yes
Bins per distance decade (log scale)	20
All sources	
Magnitude integration increment	0.1 M
Apply magnitude scaling factors	no

Chapter 5

Results

5.1 Sensitivity of the cumulative weight

This section discusses the cumulative weight distributions that are used to calculate the ground respose spectra (GRS). Figure 5.1 shows the weight accumulation for the PGA and spectral frequencies f = 40, 33, 20, 10 and 5 Hz at AFE = 10^{-5} a^{-1}. Normalized weight accumulations from branches with different GMPEs were included in figure 5.1 to study the contribution of the GMPEs.

It is apparent that the modified G16 and Dahle GMPEs span over a significantly larger range of SA values compared to the Pezeshk and Fennoscandian GMPEs. The accelerations computed with the newly included GMPEs also extend to distinctively high values, e.g. up to PGA = 0,70 g (mod. G16) and 0,65 g (mod. Dahle), although the associated weight is small. PGA with respect to cumulative weight for the modified G16 and Dahle GMPEs remains below the Pezeshk GMPE nearly for the entire weight range. SA as a function of weight for the new GMPEs exceed the Pezeshk GMPE at low spectral frequencies, as seen for f = 5 - 10 Hz in figure 5.1. SA values from the FGMPE remain below the Pezeshk GMPE at every fractile as the FGMPE is essentially scaled from the Pezeshk GMPE.

It is important to understand the link between the GM predicted by the GMPEs (see section 4.2) and the GM response at the site computed with the seismic hazard analyses. The peak ground response from the Pezeshk GMPE from the hazard analyses in figure 5.1 was considered unexpectedly high compared to the GMPE values in figure 4.5. This raises concerns about

the use of the Pezeshk GMPE below its range of applicability ($M_w < 5,0$), where the GMPE obtains considerably high GM values (see figure 4.6). The concern is supported by the hazard deaggregation presented in [11], where the mean magnitude for PGA = 0,20 g was as low as $M_w = 2,39$. Unfortunately, the effect of the GMPEs on hazard analyses is so complicated that it is impossible to draw conclusions without further deaggregation study including multiple logic tree branches.

Figure 5.2 shows the total weight accumulation and the normalized weight accumulation of the different $m_{\max}$ branches (see figure 4.8) for the PGA. Based on figure 5.2, the $m_{\max}$ values and weights should be selected with consideration, as an interval of $\Delta m_{\max} = 0,5$ can cause differences above 0,1 g for a given fractile. The low total weight of the $m_{\max} = 6,5$ and 7,0 branches ($w(m_{\max} = 6,5 \text{ and } 7,0) = 0,056$) prompted us to study the effect of excluding these branches from the PGA calculation. Table 5.1 shows the normalized PGA values calculated with only branches $m_{\max} = 5,5$ and 6,0. Excluding the high-magnitude branches systematically decreased the PGA with changes up to 11,6% observed in table 5.1.

Table 5.1: Normalized PGA values calculated at different fractiles with only branches $m_{\max} = 5,5$ and 6,0. The difference from the total PGA value is given in the brackets.

fractile	AFE = 10^{-5} a^{-1} (g)	AFE = 10^{-7} a^{-1} (g)
5%	0,0471 (-2,16%)	0,343 (0,0%)
15%	0,0568 (-0,0%)	0,390 (0,0%)
50%	0,130 (-11,6%)	0,683 (-4,65%)
85%	0,256 (-8,6%)	1,22 (-4,98%)
95%	0,350 (-11,4%)	1,49 (-6,82%)

5.2 Ground response spectrum

In table 5.2, we present the computed spectral accelerations for a range of fractiles at AFE = 10^{-5} a^{-1}. Spectral accelerations at the other studied time frequencies (AFE = $10^{-4} - 10^{-8}$ a^{-1}) are listed in appendix C. Figure 5.3 presents the SAs in table 5.2 as a ground response spectrum (GRS). The current Hanhikivi 1 GRS [17] computed with the Pezeshk and Fennoscandian GMPEs is included for comparison.

As seen in figure 5.1, the range of acceleration values can vary significantly

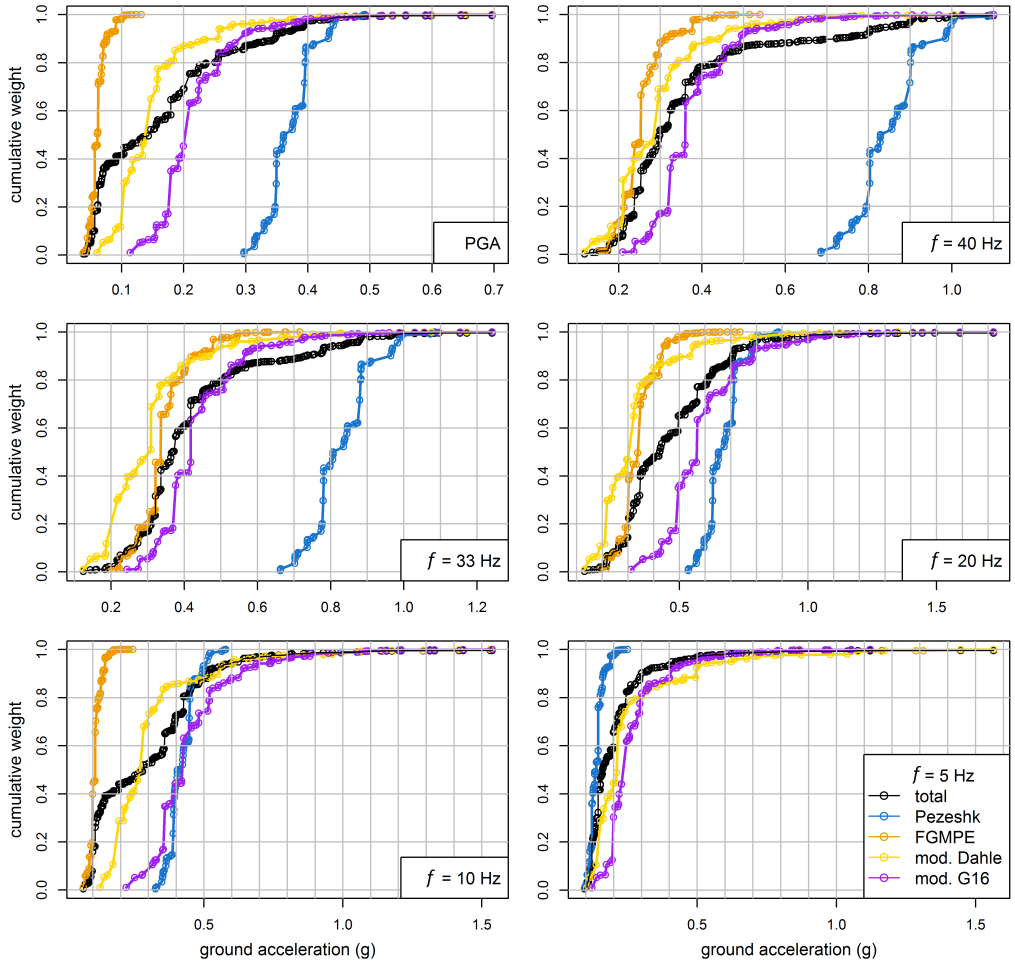

Figure 5.1: Cumulative weight as a function of acceleration plotted with the normalized cumulative weights from the GMPEs for the PGA and spectral frequencies f = 40, 33, 20, 10 and 5 Hz.

for the different GMPEs. Consequently, the GMPEs contribute to the total acceleration at different fractile ranges. As an example, the 5 and the 15% fractile GRS in figure 5.3 are mainly determined by the FGMPE, as the acceleration values resulting from the FGMPE branch are lower than the values from the other GMPE branches. For this reason, the computed 5 and 15% fractile spectra are nearly identical with the corresponsing spectra in the current Hanhikivi 1 GRS despite the presence of the new GMPEs in the logic tree.

One of the most notable features in the current Hanhikivi 1 GRS is the double-peak structure observed in the median and the fractiles below median. The double-peak structure, discussed in [17], arises from the frequency-

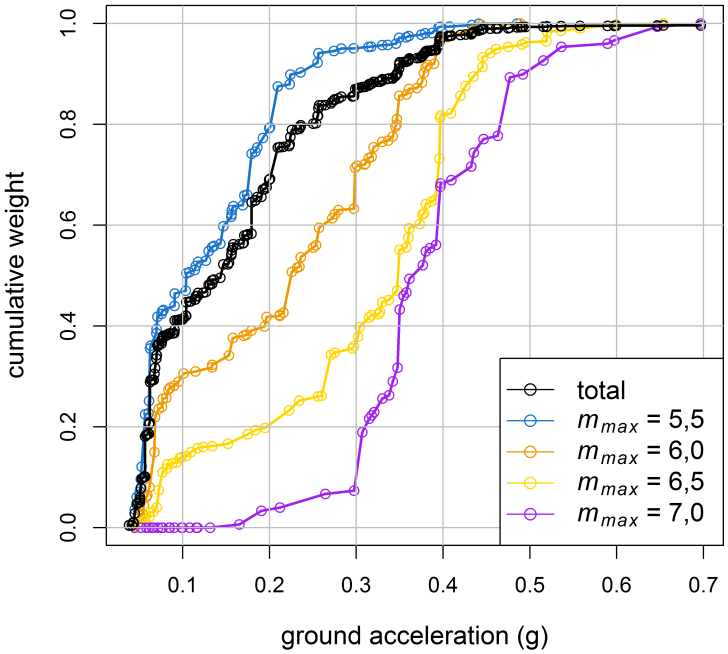

Figure 5.2: Cumulative weight as a function of peak ground response plotted with the normalized cumulative weights from the $m_{\max}$ branches in figure 4.8.

dependence in the weighting between the Pezeshk and Fennoscandian GMPEs. The structure is purely computational i.e. it is not observed in real earthquake spectra (examples of real spectra in e.g. [14]). The newly computed median spectrum does not show the double-peak structure observed in the current median. Including new GMPEs decreases the weight of the FGMPE branch increasing the median acceleration at $f \geq 10$ Hz, i.e. the range where the FGMPE is applied. When the total weight of the FGMPE branch is decreased, higher acceleration values from the G16 and Dahle GMPEs begin to contribute to the total median acceleration.

The comparison of our results to the current PSHA in figure 5.3 also shows that the 85 and 95% fractile SAs are decreased at high frequencies and increased at low frequencies with the change occurring around $f = 20$ Hz. The transition can be explained by figure 5.1, where below $f = 20$ Hz, the modified G16 and Dahle GMPEs exceed the acceleration of the Pezeshk GMPE at the 85 and 95% fractiles, whereas the Pezeshk GMPE determines the accelerations at high fractiles and frequencies. The distinctively different ranges of

the acceleration values from the Pezeshk and Fennoscandian GMPEs in the Hanhikivi 1 PSHA give rise to a large increase in amplitude at the threshold fractile of 78%, which corresponds to the total FGMPE weight [17]. In figure 5.3 (dashed line), the substantial increase of 114% between the maximum median and the maximum 85% fractile amplitudes can be attributed to this threshold effect. Including the new GMPEs makes the GRS less sensitive to the changes in the weight ratio between the Pezeshk and the Fennoscandian GMPEs.

Table 5.2: Spectral accelerations computed for an annual frequency of exceedance of 10^{-5} a^{-1}. The fractiles are approximated from the total cumulative weight in figure 5.1.

frequency (Hz)	5%	15%	50%	85%	95%
PGA	0,0482	0,0568	0,147	0,280	0,395
40	0,193	0,220	0,299	0,495	0,858
33,33	0,222	0,279	0,369	0,548	0,845
25	0,237	0,330	0,425	0,682	0,792
20	0,219	0,303	0,423	0,651	0,785
10	0,0876	0,0992	0,283	0,455	0,643
6,67	0,195	0,221	0,268	0,349	0,520
5	0,111	0,122	0,161	0,262	0,435
2,5	0,0378	0,0428	0,0688	0,137	0,235
1	0,00769	0,00844	0,0126	0,0293	0,0571
0,5	0,00122	0,00184	0,00273	0,00959	0,0178

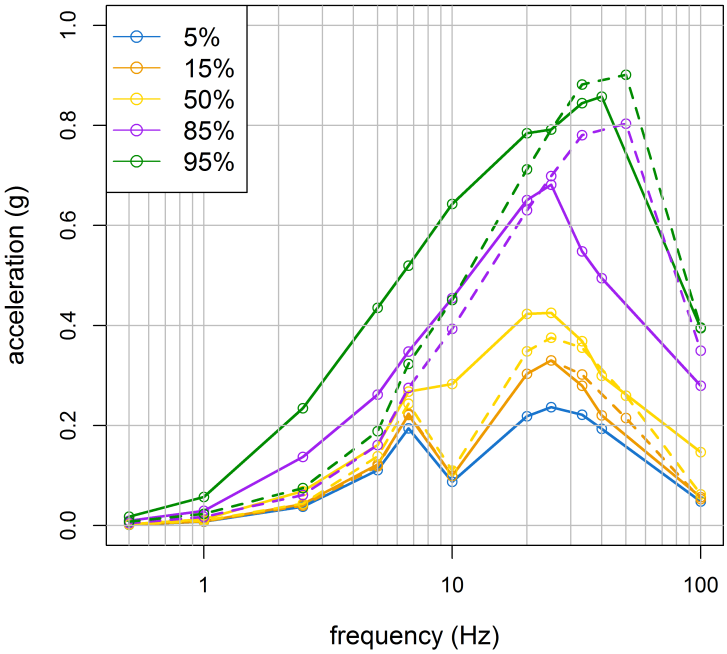

Figure 5.3: Ground response spectrum at AFE = 10^{-5} a^{-1}. The solid line illustrates the SA values shown in table 5.2, while the dashed line represents the SA values computed for the current Hanhikivi 1 PSHA [17]. The PGA is plotted at $f = 100$ Hz.

Chapter 6

Conclusions

In this work, we reviewed the logic tree parameters and the hazard calculation in the current Hanhikivi 1 PSHA. The work was largely based on prior PSHA reports [15–17] with a focus on the maximum magnitude and the GMPE parameters. It should be noted that the results presented here are only for sensitivity analysis with the purpose to support the previous reports.

We began by reviewing the current $m_{\max}$ weight assessment introduced in [11]. The assessment process repeated with the parameters in [11] resulted in different weight factors. We corrected the weighting, but the error was so small that the correction was negligible. While the highest considered $m_{\max}$ in the logic tree is based on literature, the choice of the lowest considered $m_{\max}$ is arbitrary. In light of this, we attempted to include a maximum magnitude of $M_w = 5{,}0$ in the logic tree. The resulting weight, $W(m_{\max}) = 0{,}86$, was deemed overly optimistic and excluded. Our attempt demonstrates the weakness in the current approach; it is very sensitive to the ambiguously chosen lowest considered magnitude. In pursuit of a less sensitive method, we attempted to directly derive the maximum magnitude and its standard deviation instead of the current method of assessing confidence levels. This approach resulted in $m_{\max} = 4{,}43 \pm 0{,}51$, which was unreasonably low. The method was originally applied for the seismically active western NA and appears to fail when applied to a less active area. All in all, our efforts with maximum magnitude have only managed to emphasize the issues regarding weight assessment.

We included two new GMPEs in the current Hanhikivi 1 logic tree. The first GMPE, namely the modified G16 GMPE, was recently derived in cooperation with the Finnish nuclear industry [2]. The second GMPE was derived

from the Dahle function and calibrated to the Fennoscandian data in this thesis. The Dahle function was selected as the base model, because it had been applied at the Hanhikivi site [7] and the Loviisa site [39]. The GMPE comparison in section 4.2 showed that the GMPEs predicted comparable GM values in the $R_{\text{hyp}} = 10$ - 100 km range, but predicting ground motion below $R_{\text{hyp}} = 10$ km is a challenging task due to the scarcity of the calibration data. A comparison between the modified Dahle GMPE, the measurements and the other GMPEs suggests that the modified Dahle GMPE underestimates ground motion for $M_w < 5,0$ in near distance ($R_{\text{hyp}} \leq 10$ km). We decided to include the modified Dahle GMPE in the logic tree despite the shortcomings, since the GMPE is reasonable at high magnitudes. Nevertheless, we assigned the modified Dahle GMPE a lower weight than for the modified G16 following the discussion above. Weight assessment of the GMPEs is difficult as the uncertainty is epistemic. Furthermore, the reliability often depends on spectral frequency and magnitude. Fortunately, the weighting of the logic tree branches is also easily changed in PSHA.

We run the seismic hazard analyses on EZ-FRISK and compiled the weight accumulation functions according to the logic tree. In section 5.1, we showed the weight accumulation computed with the entire logic tree and compared it to the accumulation computed with the normalized GMPE and maximum magnitude branches. Unfortunately it is impossible to draw further conclusions on how the GMPEs affect the hazard analysis results without further magnitude and distance deaggregation studies. Updated deaggregation studies would also help to define the significant distance and magnitude ranges. For example, the Pezeshk GMPE was applied beyond its range of applicability ($M_w < 5$) possibly leading to inconsistently high amplitudes. Section 5.1 also presents the sensitivit study for the maximum magnitude. The sensitivity study showed that estimating the cumulative weight with only branches $m_{\text{max}} = 5{,}5$ and 6,0 decreased the values by up to 12% between the 5 - 95% fractiles. It could be feasible to neglect the high-magnitude branches as the difference is small considering the overall uncertainty in PSHA and the number of required hazard analyses would reduce by half. Lastly, it should be noted that our analyses assume a focal depth of $d = 45$ km, while $d = 30$ km could be more realistic, although the effect is expected to be small as explained in section 2.

The computed cumulative weight functions were compiled into ground response spectra for a range of annual frequencies of exceedance (AFE = 10^{-4} a^{-1} - 10^{-8} a^{-1}). In section 5.2, we focus on the GRS at AFE = 10^{-5} a^{-1} due to its safety significance and compare it to the current Hanhikivi 1 GRS. In general, the drastically different ranges of the Pezeshk and Fennoscandian

GMPEs result in some unphysical features in the current Hanhikivi 1 PSHA. These features include the double-peak structure and the large increase in the amplitude around the threshold fractile of 76%. Including the new GMPEs in the PSHA makes the GRS less sensitive to the changes in the weight ratio between the Pezeshk and the Fennoscandian GMPEs alleviating these purely computational features.

In summary, we studied the sensitivity of the GRS to the $m_{\max}$ and GMPE parameters. We managed to improve our understanding of these parameters, but our work also brought up issues regarding them. We encountered problems in the current maximum magnitude assessment, which we could not solve. Including new GMPEs in the logic tree diminished the problems recognized in the current PSHA. Unfortunately, the challenge of defining the included GMPEs will remain for as long as there is a lack of data in the critical magnitude and distance range.

Bibliography

[1] Säteilyturvakeskus (STUK). Ohje YVL B.7, Varautuminen sisäisiin ja ulkoisiin uhkiin ydinlaitoksessa, 2013.

[2] L.A. Fülöp, V. Jussila, R. Aapasuo, T. Vuorinen, and P. Mäntyniemi. A Ground-Motion Prediction Equation for Fennoscandian Nuclear Installations. *SAFIR2018 - The Finnish Research Programme on Nuclear Plant Safety 2015-2018 Final Report, VTT Technology*, 349:422–433, 2019.

[3] A. Dahle, H. Bungum, and K.B. Kvamme. Attenuation Models Inferred from Intraplate Earthquake Recordings. *Earthquake Engineering and Structural Dynamics*, 19:1125–1141, 1990.

[4] Radiation and Nuclear Safety Authority STUK. Radiation and nuclear safety authority regulation on the safety of nuclear power plant, Regulation STUK Y/1/2018.

[5] Fennovoimassa ei säikähdetty poikkeuksellisen suurta järistystä: "Ei olisi vaikuttanut edes sähköntuotantoon", 2016. From https://yle.fi/uutiset/3-8757409.

[6] P. Mäntyniemi. Assessment of seismicity and design earthquake to possible nuclear power plant sites in Pyhäjoki, Ruotsinpyhtää and Simo according to the YVL 2.6 regulations. Technical report, Institute of Seismology, University of Helsinki, 2008. FH1-00006586.

[7] J. Saari, P. Heikkinen, and P. Varpasuo. Estimation of seismic hazard in territory of Finland. Technical report, ÅF-Consult Ltd, 2009. FH1-00006589.

[8] J. Saari and M. Malm. Complementary calculations related to seismic hazard of the potential nuclear power plant sites in Pyhäjoki and Simo. Technical report, ÅF-Consult Ltd, 2010.

[9] Yle. Fennovoman ydinvoimala tulee Pyhäjoelle, 2011. From https://yle.fi/uutiset/3-5433404.

[10] Selvityspyyntö 1/J42219/2010: Fennovoiman ydinvoimalaitoshanke, seismiset suunnitteluarvot., 2011. CR-02-0000267.

[11] J. Saari, B. Lund, M. Malm, K. Oinonen P. Mäntyniemi, T. Tiira, M. Uski, and T. Vuorinen. Evaluating Seismic Hazard for the Hanhikivi Nuclear Power Plant Site - Seismological Characteristics of the Seismic Source Areas, Attenuation of Seismic Signal, and Probabilistic analysis of Seismic Hazard. Technical report, ÅF-consult, 2015.

[12] A. Korja and E. Kosonen. Seismotectonic framework and models in the northern part of the Fennoscandian shield. Technical report, Faculty of Science, University of Helsinki, Finland, 2015.

[13] V. Jussila, B. Falth, B. Lund, J. Saari, P. Voss, J. Puttonen, and L. Fülöp. Decreasing uncertainty in seismic hazard estimates in Fennoscandia by use of seismic sourve modeling. *ATS Ydintekniikka*, 46:16–22, 2017.

[14] T. Vuorinen, T. Tiira, M. Uski, and B. Lund. Updated Fennoscandian GMPE. Technical report, Institute of Seismology, University of Helsinki, 2018.

[15] M. Malm and O. Kaisko. Updated ground response spectrum for the Hanhikivi site. Technical report, ÅF-Consult Ltd, 2017. FH1-00042168.

[16] ÅF-Consult Ltd. Hanhikivi seismic hazard - 10-7/a PGA values, 2018. FH1-00046367 r1.

[17] J. Tang. Updated seismic hazard spectra for the Hanhikivi site. Technical report, Fennovoima, 2018. FH1-00053982.

[18] IAEA Safety Standards Series No. SSG-9. Seismic hazards in site evaluation for nuclear installations. Technical report, IAEA, Vienna, 2010.

[19] J. Helander. Seismic design basis of Hanhikivi 1. Technical report, Fennovoima, 2018. FH1-00004885.

[20] P. Mäntyniemi, A. Kijko, and P. Retief. Parametric-historic procedure for seismic hazard assessment and its application to northern Europe. *Bolletino di Geofisica Teorica e Applicata*, 42(1-2):41–55, 2001.

[21] USNRC. Central and Eastern United States Seismic Source Characterization for Nuclear Facilities (NUREG-2115). Technical report, US Nuclear Regulatory Commission, Washington DC, 2012.

[22] P. Koskinen. Orientation of faults and their potential for reactivation in the present stress field in Finland. Master's thesis, Faculty of Science, University of Helsinki, Finland, 2013.

[23] R. Musson and H. Bungum. Logic tree of earthquake activity rates. Technical report, SHARE - Seismic Hazard Harmonization in Europe, 2011. Deliverable 3.7.

[24] O. Kaisko. Stability of the seismicity parameters b, beta and lambda - the impact of the SNSN magnitude errors. Technical report, ÅF-Consult Ltd, 2017. FH1-00042180.

[25] V. Graizer. Ground-Motion Prediction Equations for Central and Eastern North America. *Bulletin of the Seismological Society of America*, 106(4):1600–1612, 2016.

[26] B. Gutenberg and C.F. Richter. *Seismicity of the Earth and Associated Phenomena*. Princeton University Press, Princeton, New Jersey, first edition, 1949.

[27] A. Kijko. Estimation of the Maximum Earthquake Magnitude, mmax. *Pure and Applied Geophysics*, 161:1–27, 2004.

[28] H. Cramer. *Mathematical Methods of Statistics*. Princeton University Press, Princeton, 1961.

[29] N.C. Nigam and P.C. Jennings. Calculation of the response spectra from strong-motion earthquake records. *Bulletin of the Seismological Society of America*, 59(2):909–922, 1969.

[30] S. Pezeshk, A. Zandieh, and B. Tavakoli. Hybrid Empirical Ground-Motion Prediction Equations for Eastern North America Using NGA Models and Updated Seismological Parameters. *Bulletin of the Seismological Society of America*, 101(4):1859–1870, 2011.

[31] O. Kaisko and J. Mattila. Analysis of the rupture potential of a fracture zone at the Hanhikivi site. Technical report, ÅF-Consult Ltd, 2018. FH1-00052632.

[32] J.W. Baker. *Introduction to Probabilistic Seismic Hazard Analysis*. White Paper Version 2.0.1, 2013.

[33] Inc. Fugro Consultants. EZ-FRISK 7.65 Build 004 User's manual.

[34] University of California. Next Generation Attenuation Relationships for Central & Eastern North-America (NGA-East). From https://peer.berkeley.edu/research/nga-east.

[35] Western University. Ground Motion Databases. From https://www.seismotoolbox.ca/index.html.

[36] F. Scherbaum. Of poles and zeros: Fundamentals of digital seismology. *Modern approaches in geophysics*, 15, 2006.

[37] F.O. Strasser, N.A. Abrahamson, and J.J. Bommer. Sigma: Issues, Insights, and Challenges. *Seismological Research Letters*, 80(1):40–56, 2009.

[38] G.M. Atkinson and D.M. Boore. Earthquake Ground-Motion Prediction Equations for Eastern North America. *Bulletin of the Seismological Society of America*, 96(6):2181–2205, 2006.

[39] T. Leppanen, P. Varpasuo, M. Malm, and O. Kaisko. Re-evaluation of seismic hazard at Loviisa and Olkiluoto sites. Technical report, BestPSHANI2018, Cararache-Chäteau, France, May 2018.

Appendix A: Modified Dahle GMPE and measured data

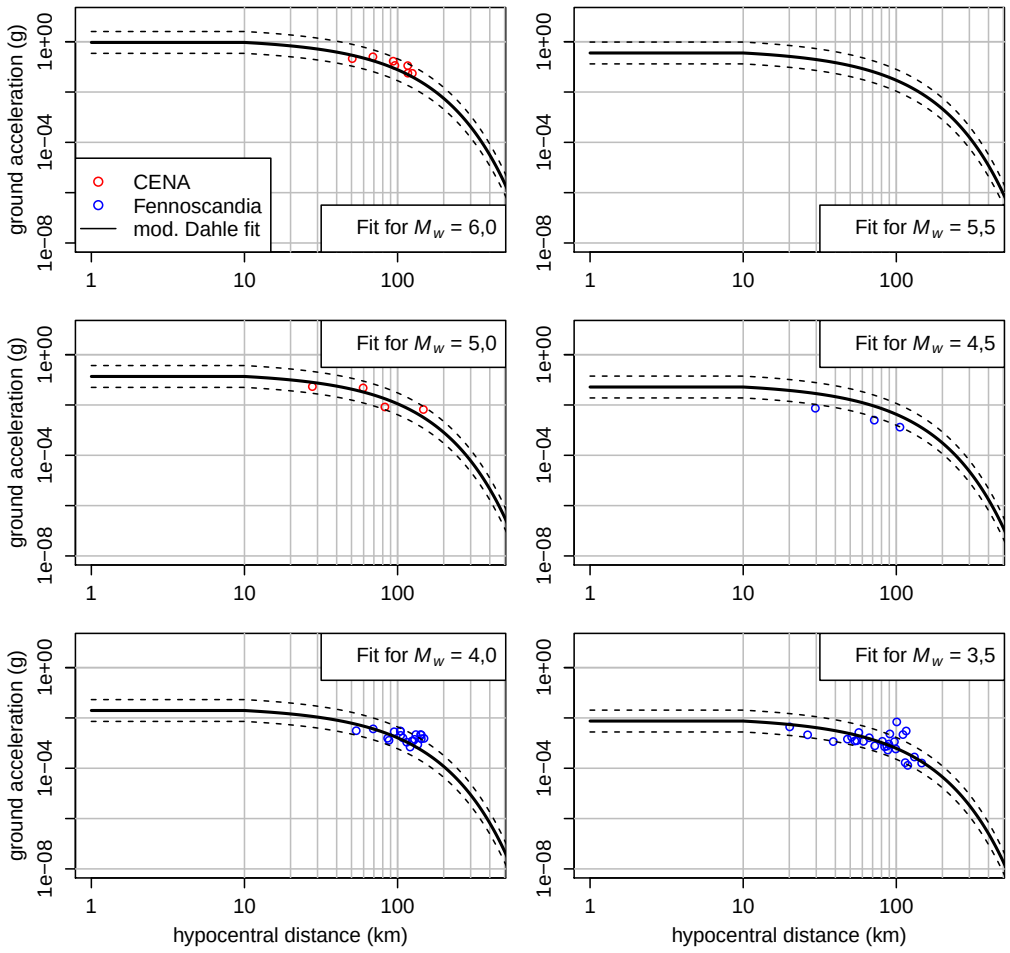

Figure 1: The modified Dahle GMPE plotted with the calibration points for spectral frequency $f = 40$ Hz. Dashed lines represent the $\overline{\lg(Y)} \pm \sigma_{\lg(Y)}$ errors. The measurements are shown in the range of $M_w \pm \Delta m$, where $\Delta m = 0,25$.

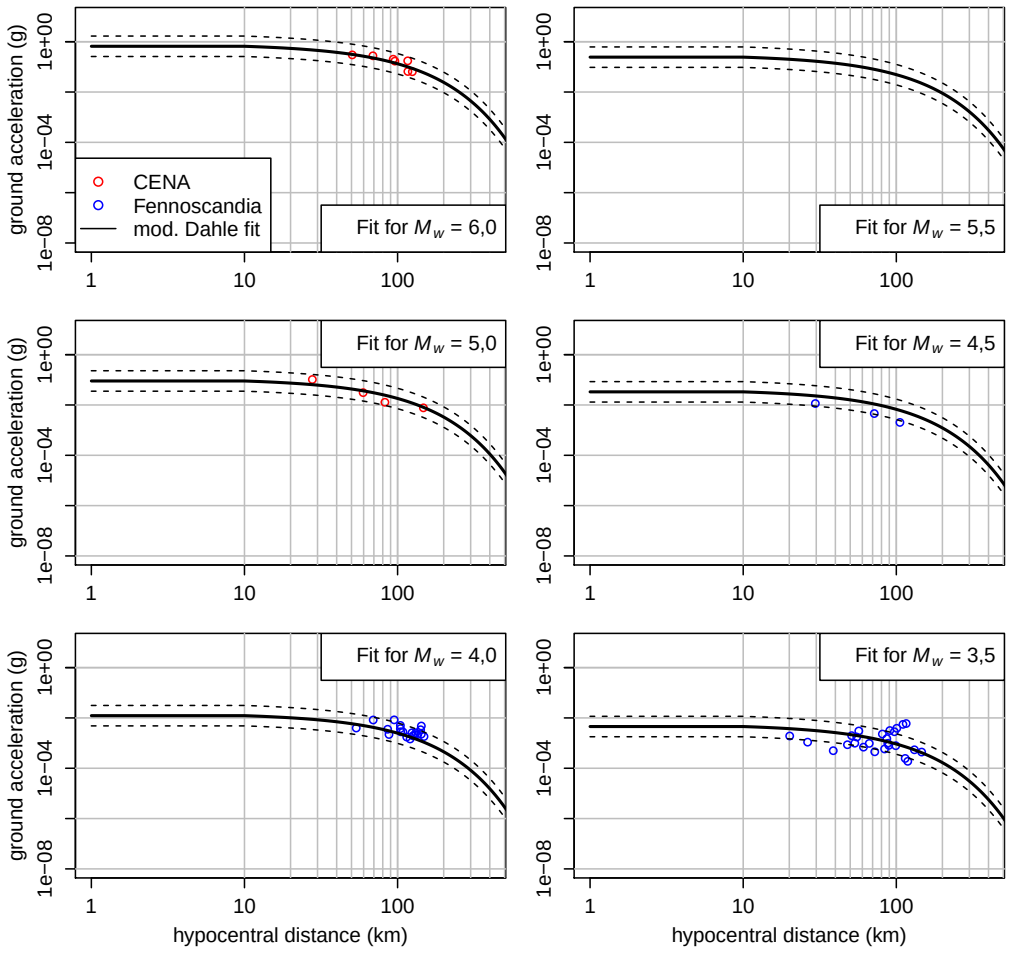

Figure 2: The modified Dahle GMPE plotted with the calibration points for spectral frequency $f = 20$ Hz. Dashed lines represent the $\overline{\lg(Y)} \pm \sigma_{\lg(Y)}$ errors. The measurements are shown in the range of $M_w \pm \Delta m$, where $\Delta m = 0,25$.

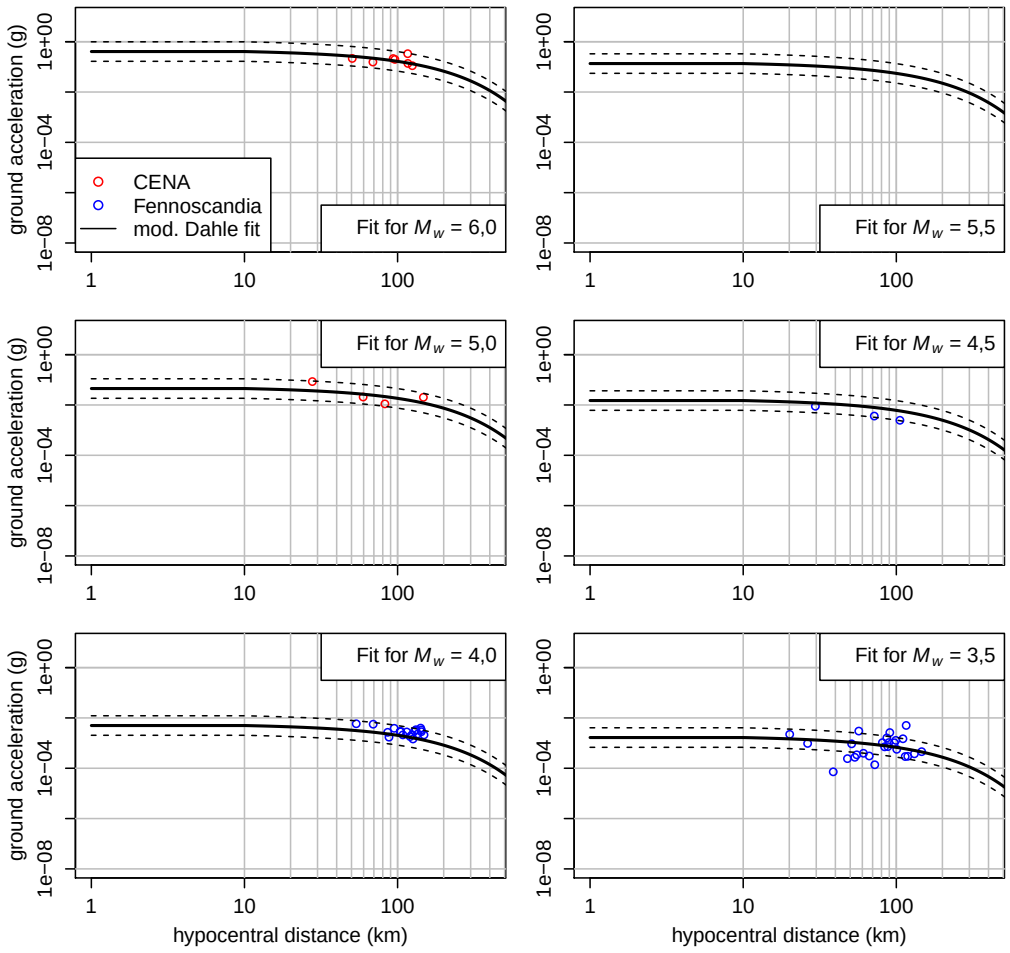

Figure 3: The modified Dahle GMPE plotted with the calibration points for spectral frequency $f = 10$ Hz. Dashed lines represent the $\overline{\lg(Y)} \pm \sigma_{\lg(Y)}$ errors. The measurements are shown in the range of $M_w \pm \Delta m$, where $\Delta m = 0,25$.

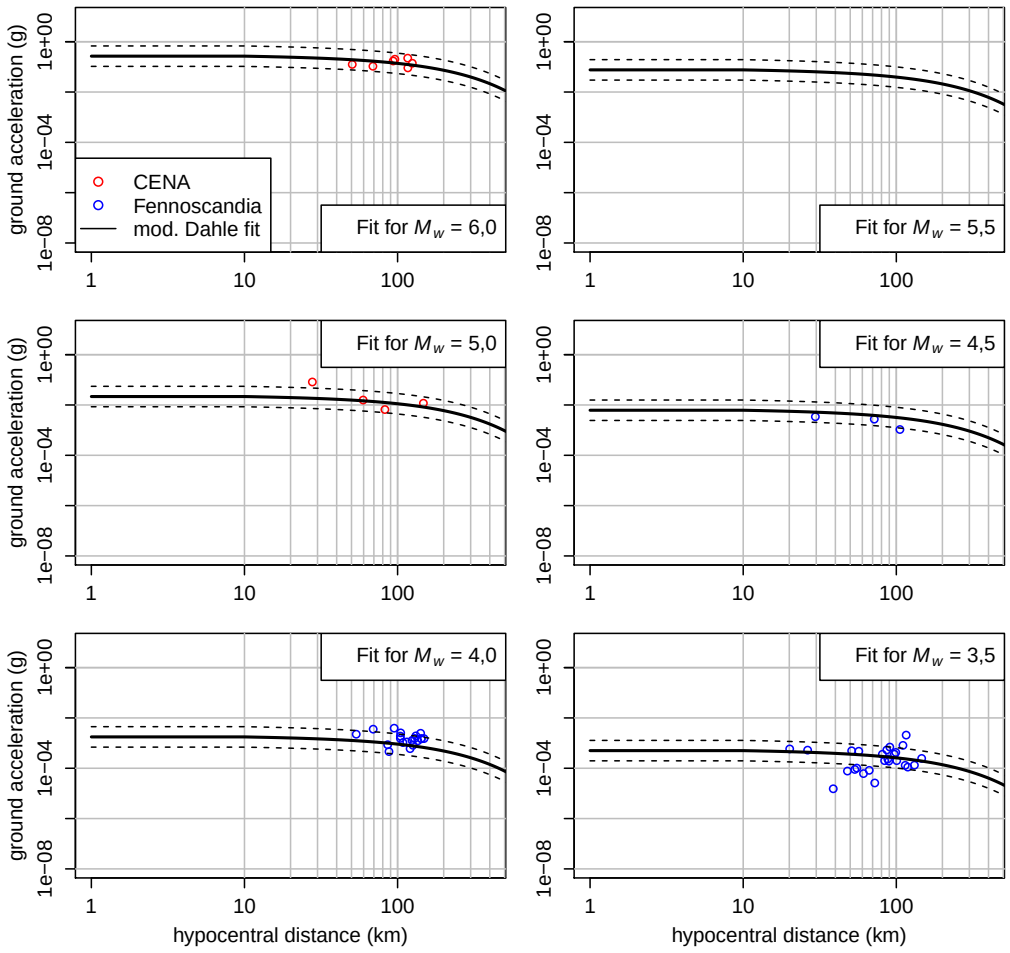

Figure 4: The modified Dahle GMPE plotted with the calibration points for spectral frequency $f = 5$ Hz. Dashed lines represent the $\overline{\lg(Y)} \pm \sigma_{\lg(Y)}$ errors. The measurements are shown in the range of $M_w \pm \Delta m$, where $\Delta m = 0,25$.

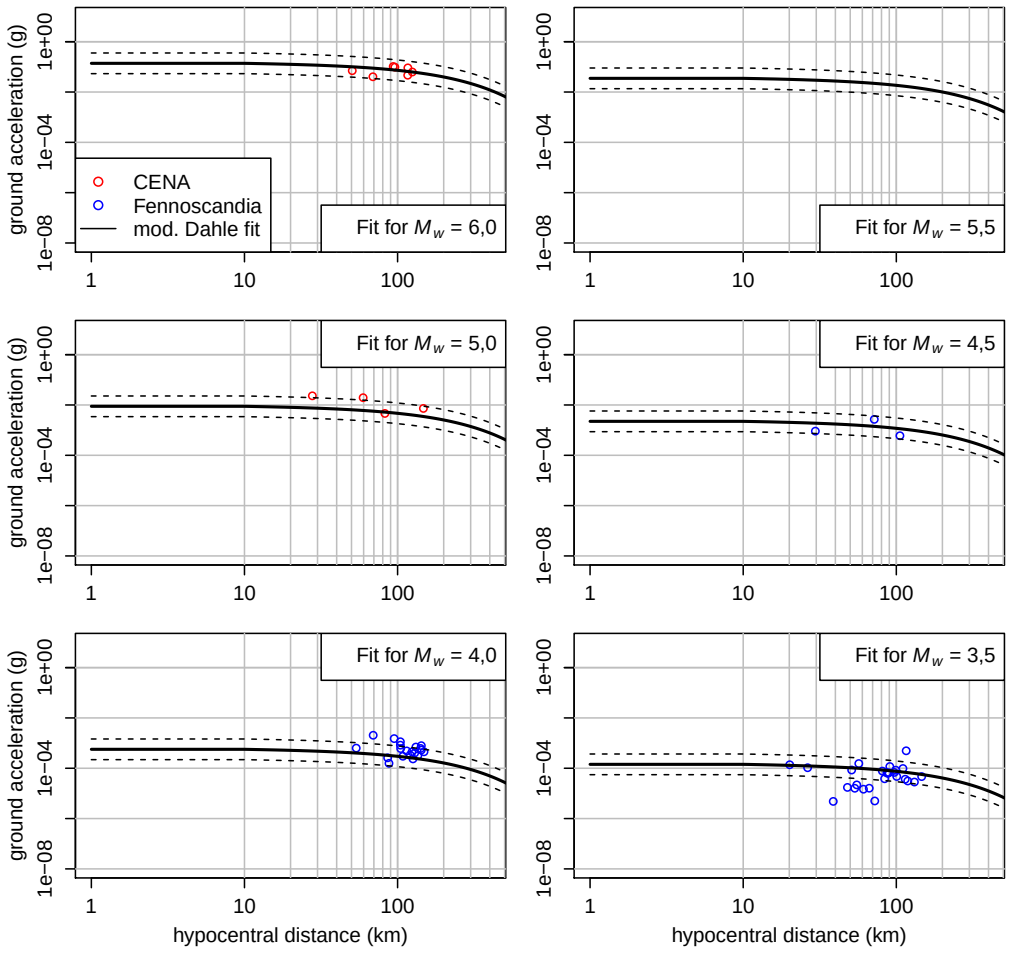

Figure 5: The modified Dahle GMPE plotted with the calibration points for spectral frequency $f = 2{,}5$ Hz. Dashed lines represent the $\overline{\lg(Y)} \pm \sigma_{\lg(Y)}$ errors. The measurements are shown in the range of $M_w \pm \Delta m$, where $\Delta m = 0,25$.

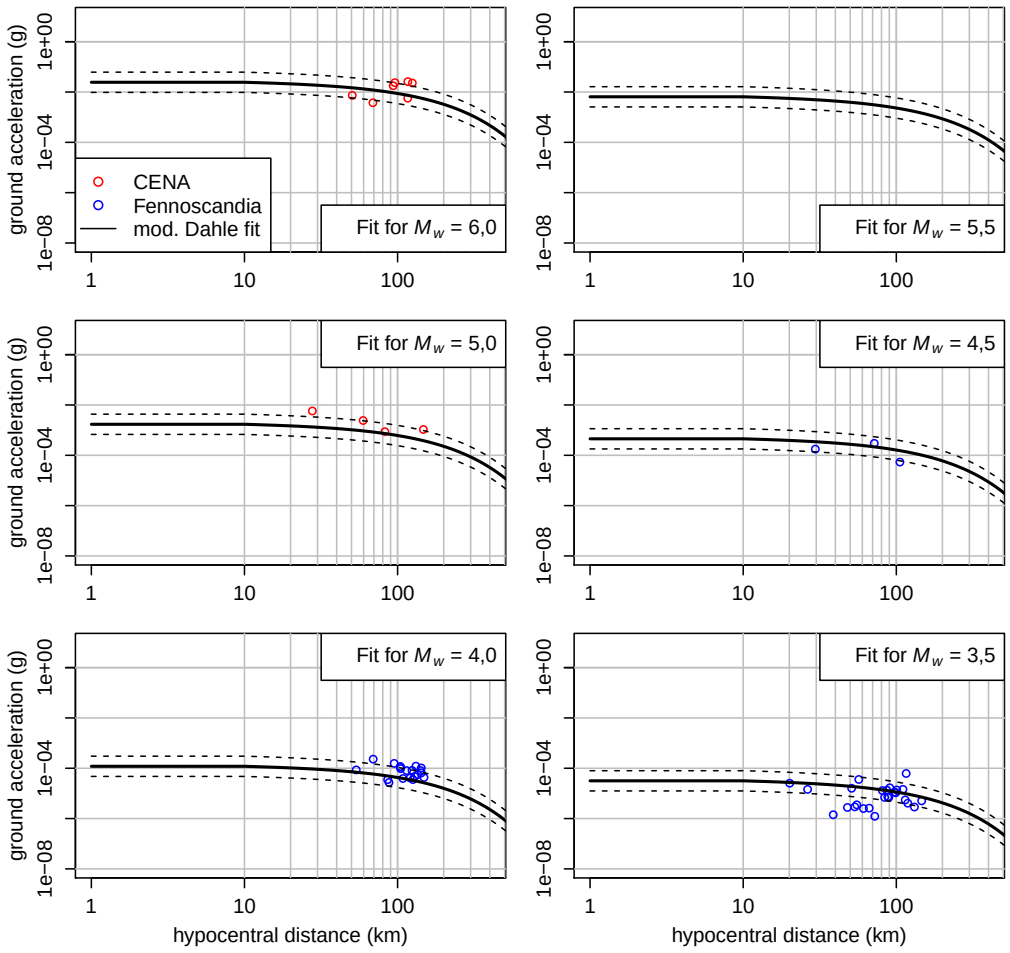

Figure 6: The modified Dahle GMPE plotted with the calibration points for spectral frequency $f = 1{,}0$ Hz. Dashed lines represent the $\overline{\lg(Y)} \pm \sigma_{\lg(Y)}$ errors. The measurements are shown in the range of $M_w \pm \Delta m$, where $\Delta m = 0,25$.

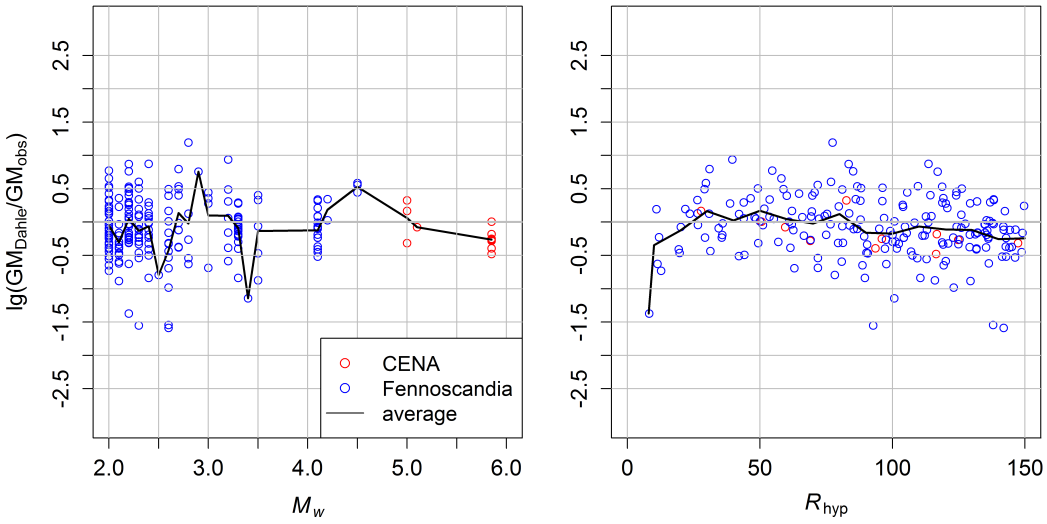

Figure 7: Deviation of the modified Dahle GMPE from the calibration data for spectral frequency $f = 40$ Hz as a function of magnitude M_w (left) and distance R_{hyp} (right). The solid line shows the average deviation.

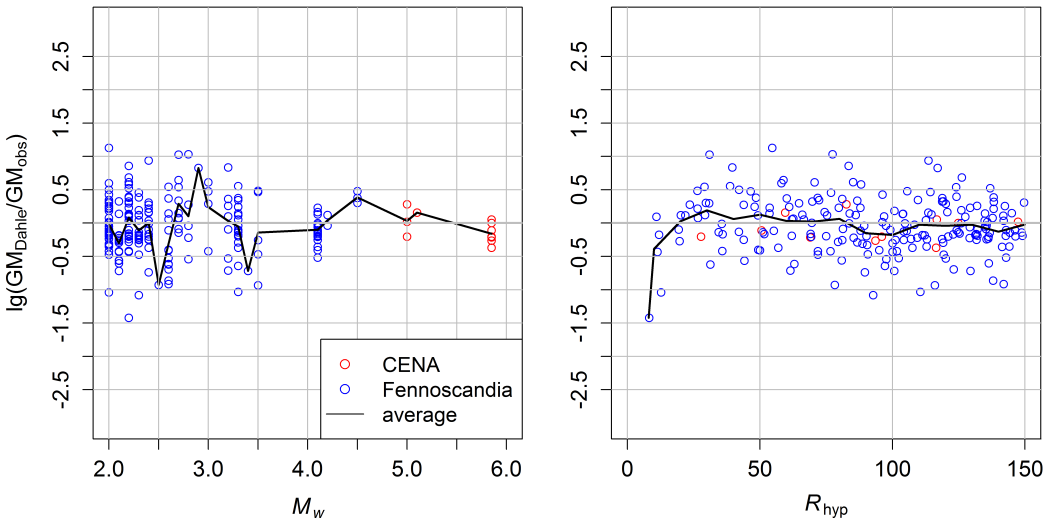

Figure 8: Deviation of the modified Dahle GMPE from the calibration data for spectral frequency $f = 20$ Hz as a function of magnitude M_w (left) and distance R_{hyp} (right). The solid line shows the average deviation.

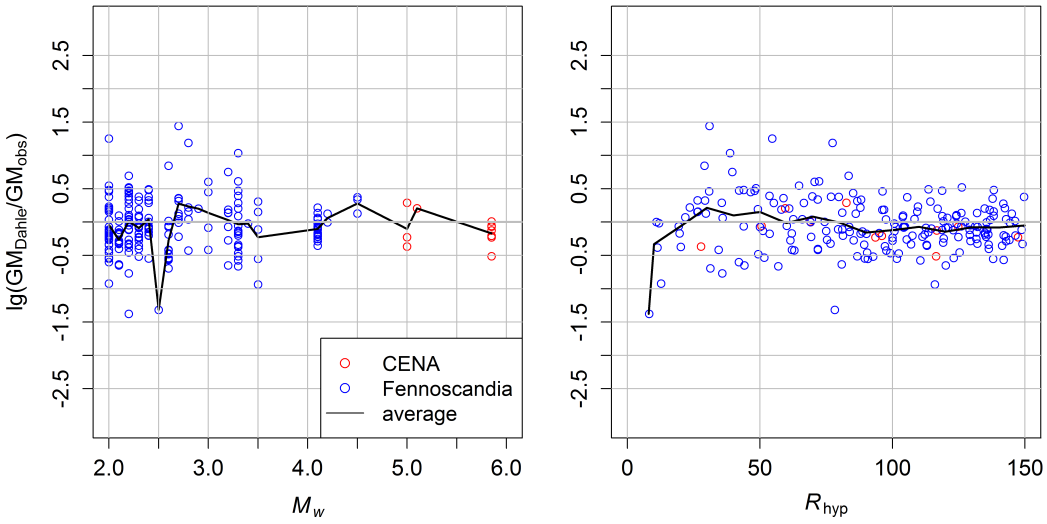

Figure 9: Deviation of the modified Dahle GMPE from the calibration data for spectral frequency $f = 10$ Hz as a function of magnitude M_w (left) and distance R_{hyp} (right). The solid line shows the average deviation.

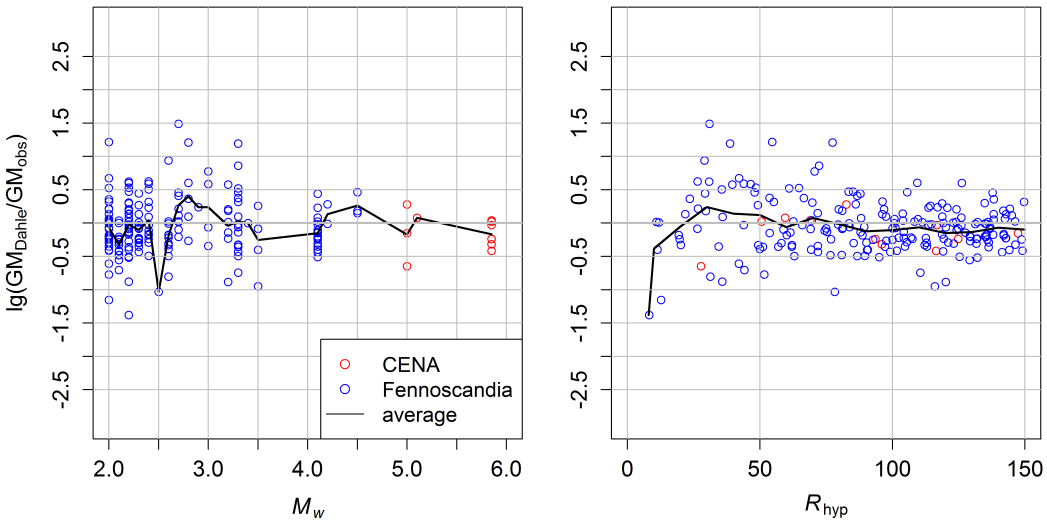

Figure 10: Deviation of the modified Dahle GMPE from the calibration data for spectral frequency $f = 5{,}0$ Hz as a function of magnitude M_w (left) and distance R_{hyp} (right). The solid line shows the average deviation.

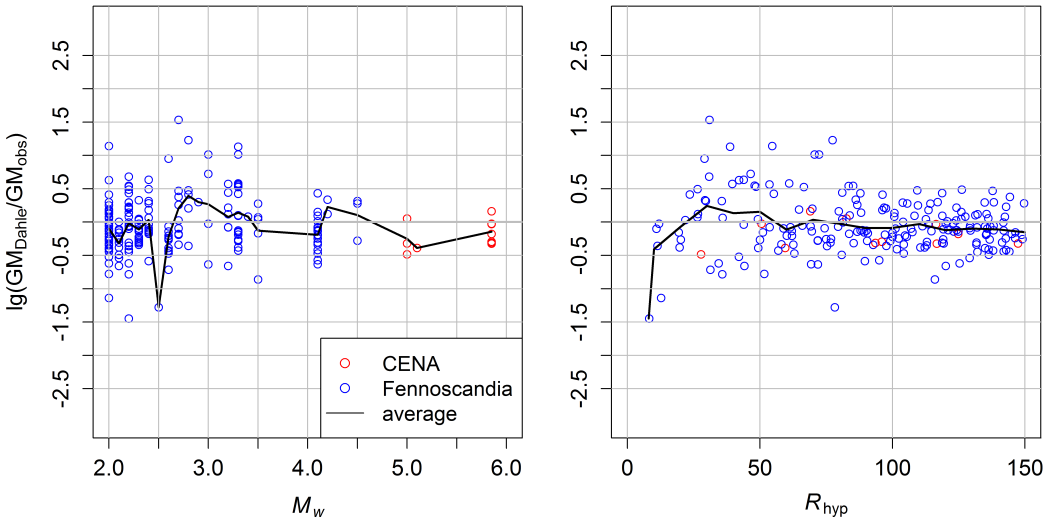

Figure 11: Deviation of the modified Dahle GMPE from the calibration data for spectral frequency $f = 2{,}5$ Hz as a function of magnitude M_w (left) and distance R_{hyp} (right). The solid line shows the average deviation.

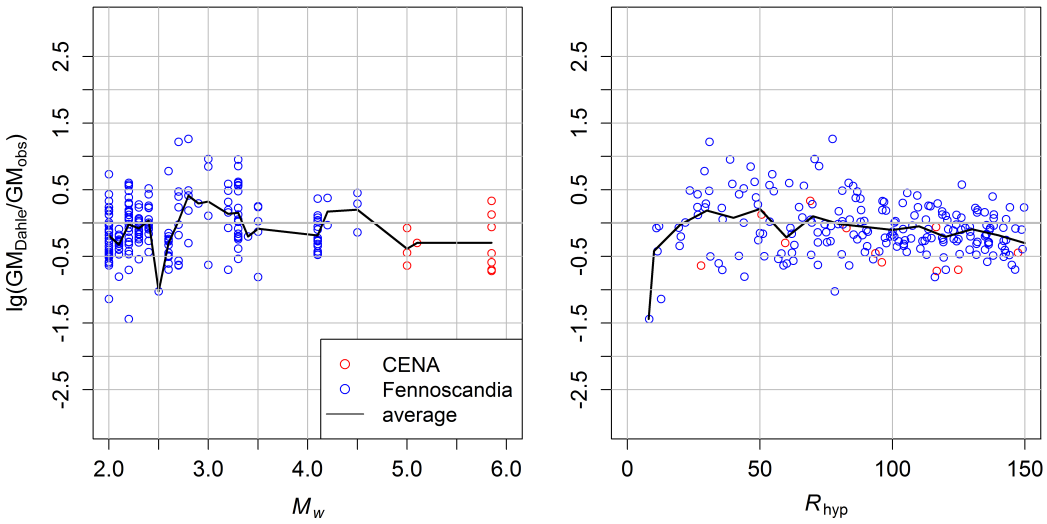

Figure 12: Deviation of the modified Dahle GMPE from the calibration data for spectral frequency $f = 1{,}0$ Hz as a function of magnitude M_w (left) and distance R_{hyp} (right). The solid line shows the average deviation.

Appendix B: GMPE comparison

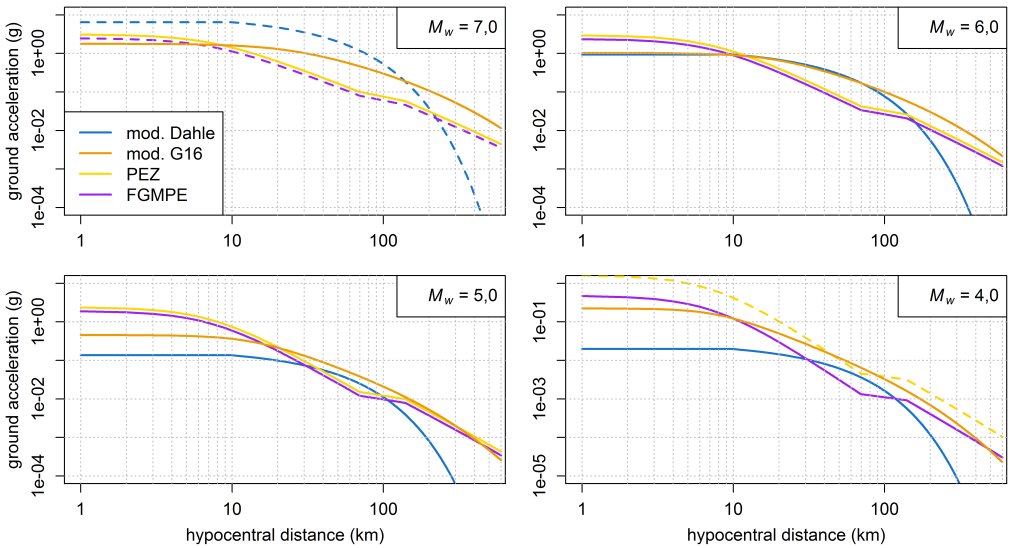

Figure 13: The GMPEs plotted between M_w = 4,0 - 7,0 for spectral frequency f = 40 Hz. Dashed line implies that the GMPE is out of its range of applicability.

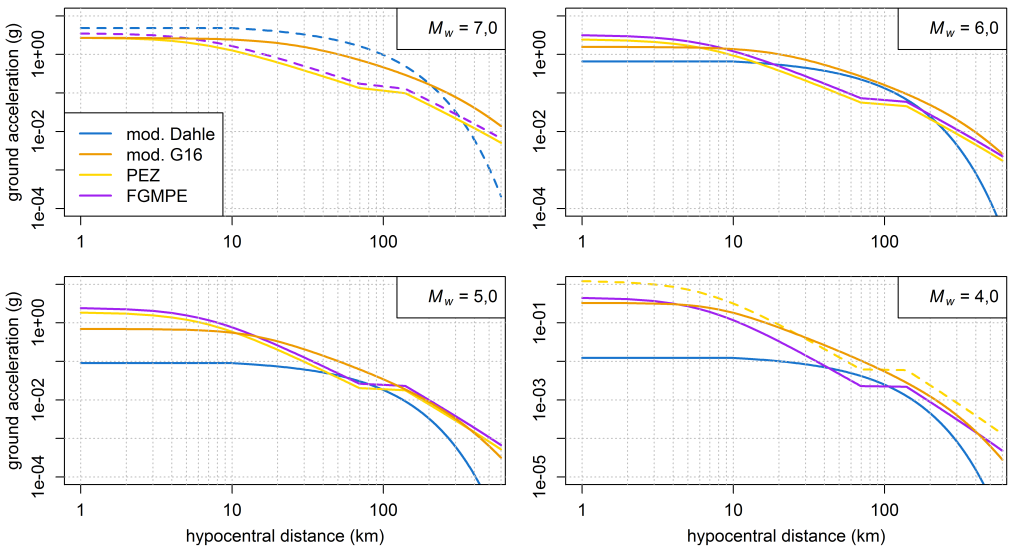

Figure 14: The GMPEs plotted between M_w = 4,0 - 7,0 for spectral frequency f = 20 Hz. Dashed line implies that the GMPE is out of its range of applicability.

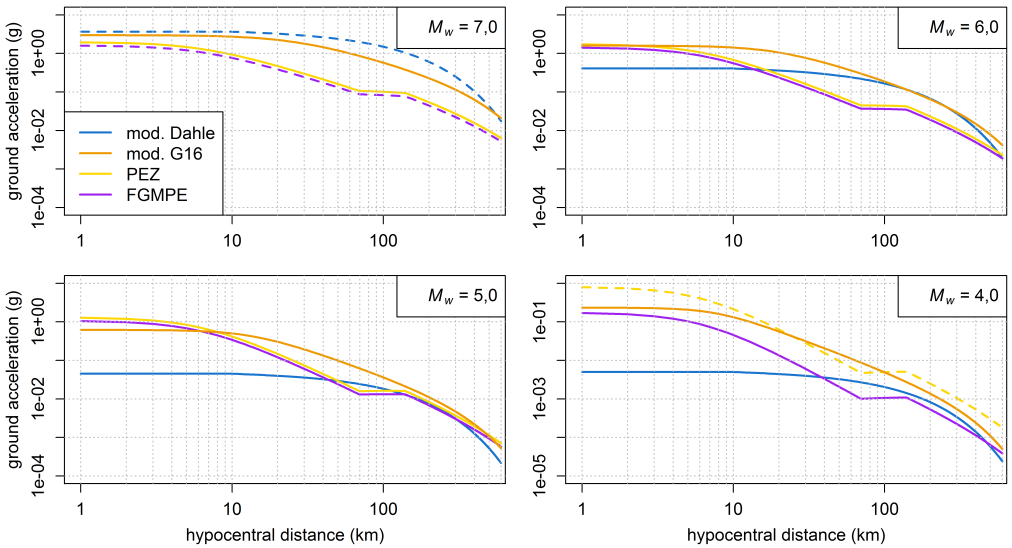

Figure 15: The GMPEs plotted between M_w = 4,0 - 7,0 for spectral frequency f = 10 Hz. Dashed line implies that the GMPE is out of its range of applicability.

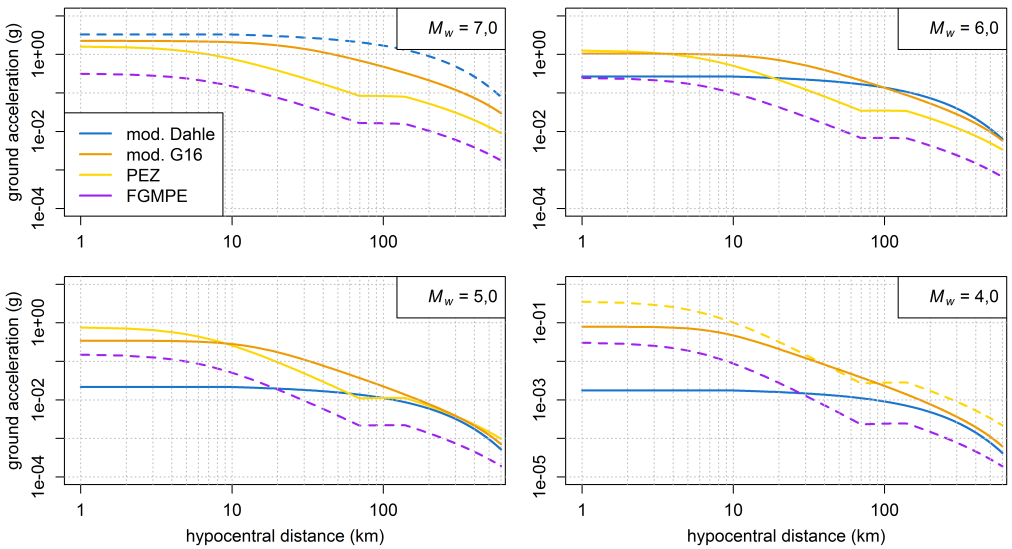

Figure 16: The GMPEs plotted between M_w = 4,0 - 7,0 for spectral frequency f = 5,0 Hz. Dashed line implies that the GMPE is out of its range of applicability.

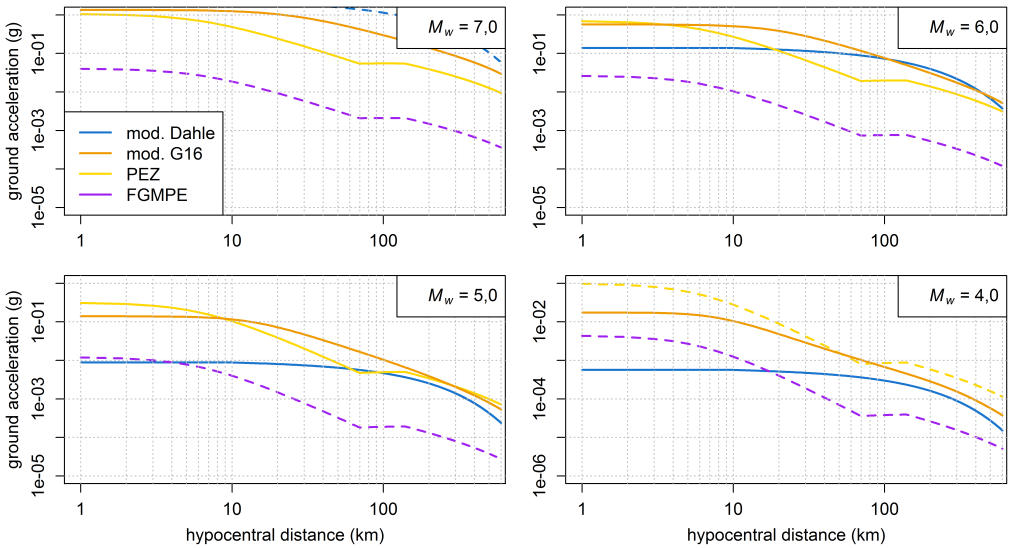

Figure 17: The GMPEs plotted between $M_w = 4{,}0$ - 7,0 for spectral frequency $f = 2{,}5$ Hz. Dashed line implies that the GMPE is out of its range of applicability.

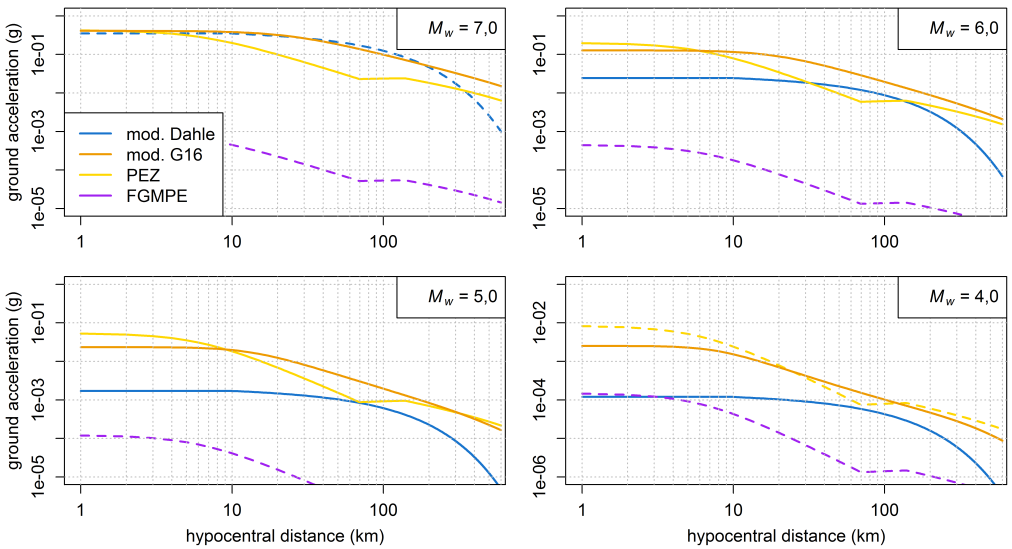

Figure 18: The GMPEs plotted between $M_w = 4{,}0$ - 7,0 for spectral frequency $f = 1{,}0$ Hz. Dashed line implies that the GMPE is out of its range of applicability.

Appendix C: Ground response spectra

Table 1: SA values computed at AFE = 10^{-4} a^{-1}. The GRS is shown in figure 19.

frequency (Hz)	5%	15%	50% (R)	85%	95%
PGA	0,0175	0,0203	0,0488	0,108	0,140
40	0,0607	0,0737	0,105	0,182	0,313
33,33	0,0662	0,10	0,132	0,212	0,306
25	0,0763	0,113	0,163	0,247	0,294
20	0,0791	0,109	0,162	0,246	0,297
10	0,0382	0,0449	0,109	0,183	0,243
6,67	0,0750	0,0808	0,0952	0,136	0,199
5	0,0460	0,0527	0,0655	0,110	0,164
2,5	0,0166	0,0185	0,0284	0,0552	0,0917
1	0,00304	0,00403	0,00574	0,0114	0,0206
0,5	0,000455	0,000804	0,00131	0,00367	0,00617

Table 2: SA values computed at AFE = 10^{-6} a^{-1}. The GRS is shown in figure 20.

frequency (Hz)	5%	15%	50% (R)	85%	95%
PGA	0,128	0,143	0,331	0,646	0,858
40	0,550	0,616	0,799	1,28	1,83
33,33	0,588	0,719	0,926	1,52	1,84
25	0,623	0,774	1,08	1,52	1,75
20	0,571	0,703	0,981	1,46	1,71
10	0,187	0,214	0,598	1,02	1,30
6,67	0,431	0,510	0,601	0,767	1,16
5	0,260	0,288	0,384	0,578	0,962
2,5	0,0791	0,0861	0,151	0,293	0,537
1	0,0151	0,0175	0,0269	0,0593	0,119
0,5	0,00279	0,00364	0,00593	0,0209	0,0432

Table 3: SA values computed at AFE = 10^{-7} a^{-1}. The GRS is shown in figure 21.

frequency (Hz)	5%	15%	50% (R)	85%	95%
PGA	0,128	0,143	0,331	0,646	0,858
40	0,550	0,616	0,799	1,28	1,83
33,33	0,588	0,719	0,926	1,52	1,84
25	0,623	0,774	1,08	1,52	1,75
20	0,571	0,703	0,981	1,46	1,71
10	0,187	0,214	0,598	1,02	1,30
6,67	0,431	0,510	0,601	0,767	1,16
5	0,260	0,288	0,384	0,578	0,962
2,5	0,0791	0,0861	0,151	0,293	0,537
1	0,0151	0,0175	0,0269	0,0593	0,119
0,5	0,00279	0,00364	0,00593	0,0209	0,0432

Table 4: SA values computed at AFE = 10^{-8} a^{-1}. The GRS is shown in figure 22.

frequency (Hz)	5%	15%	50% (R)	85%	95%
PGA	0,850	0,939	1,39	2,38	2,81
40	2,62	2,81	4,62	6,72	7,44
33,33	2,57	3,04	5,08	8,16	9,07
25	2,43	4,01	5,27	7,53	9,26
20	2,17	3,60	4,70	6,18	8,43
10	1,10	1,20	2,14	3,48	4,56
6,67	1,53	1,80	2,14	2,79	3,94
5	1,08	1,25	1,48	2,01	3,21
2,5	0,394	0,428	0,646	0,990	1,82
1	0,0648	0,0758	0,111	0,201	0,381
0,5	0,00877	0,0148	0,0261	0,0774	0,162

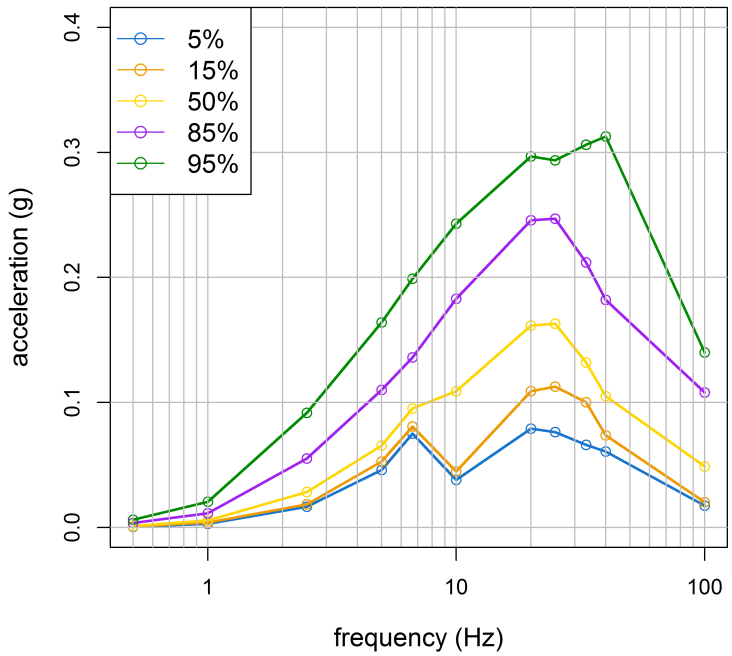

Figure 19: Ground response spectrum at AFE = 10^{-4} a^{-1}.

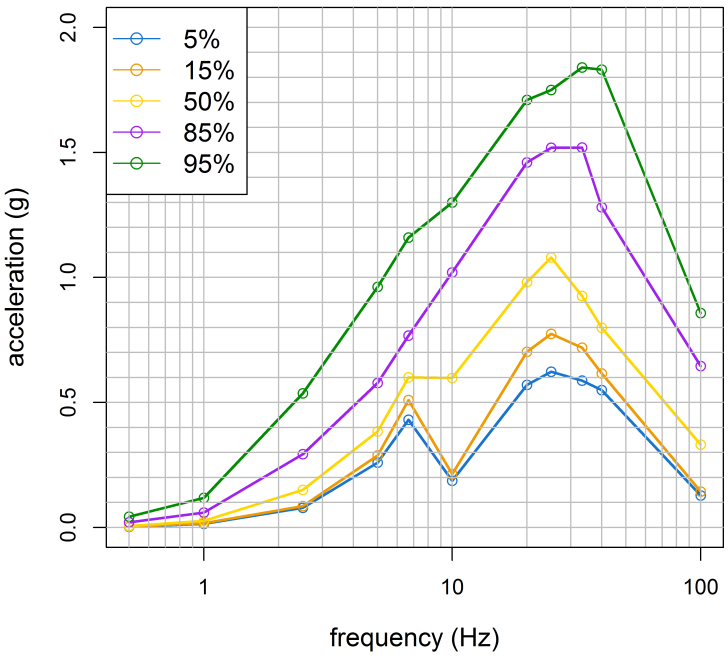

Figure 20: Ground response spectrum at AFE = 10^{-6} a^{-1}.

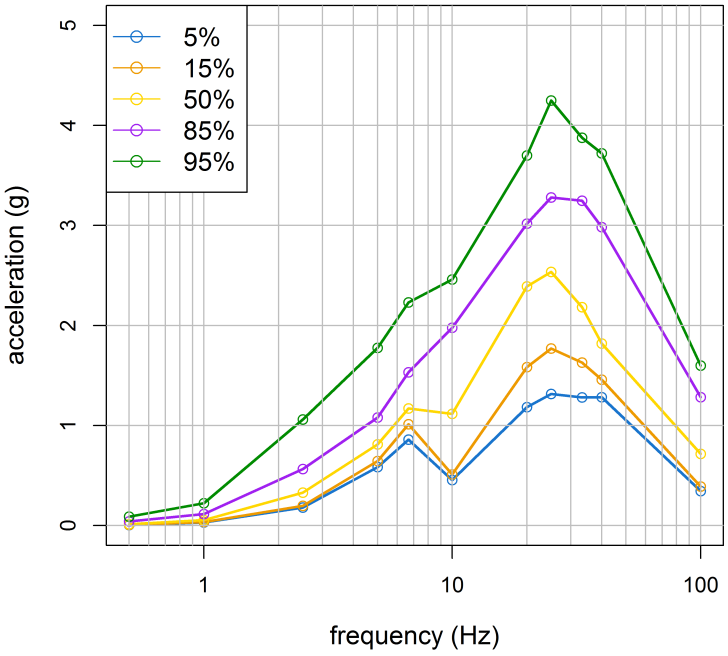

Figure 21: Ground response spectrum at AFE = 10^{-7} a^{-1}.

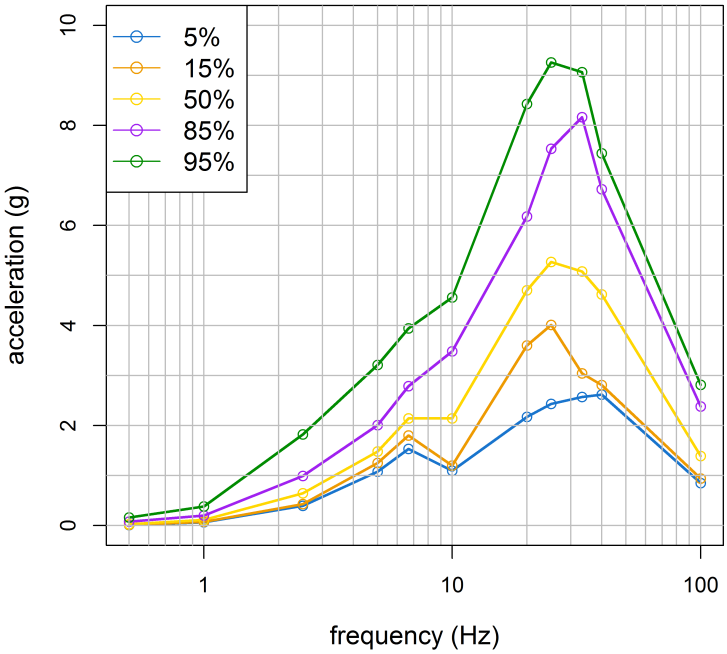

Figure 22: Ground response spectrum at AFE = 10^{-8} a^{-1}.